Environmental Research 256 (2024) 119190

Contents lists available at ScienceDirect

Environmental Research

journal homepage: www.elsevier.com/locate/envres

Towards the valorisation of glycerol by designing the surface chemistry of carbon xerogels by doping and oxygen functionalization

Naila Gómez González [a], Samantha L. Flores-López [b], Luis E. Cadus [a], Ana Arenillas [b,*], María R. Morales [a,**]

[a] Chemical Technology Research Institute (INTEQUI-CONICET), National University of San Luis (UNSL), Faculty of Chemistry, Biochemistry and Pharmacy, Almirante Brown 1455, Capital, 5700, San Luis, Argentina
[b] Instituto de Ciencia y Tecnología Del Carbono, INCAR-CSIC, Francisco Pintado Fe, 26, 33011, Oviedo, Spain

ARTICLE INFO

Keywords:
Doped carbon xerogels
Oxygen functionalities
Glycerol
Copper
Nitrogen
Silica
Graphene oxide

ABSTRACT

Research on innovative approaches to the valorisation of glycerol as a subproduct of biodiesel production has acquired an increasing demand in the development of a circular economy around energy generation, especially, in the line of improvement of the heterogeneous metallic catalysts used. In this regard, carbon xerogels have gained importance due to their stability and modifiability, while transition metals such as copper stand out as a cost-effective alternative, resulting in a technology where surface engineering plays a crucial role in achieving competitive catalytic activity. Building upon this, current research evaluates doped xerogels (Si, N, or GO) as supports of Cu and catalysts by themselves for glycerol oxidation. Benefits from the incorporation of oxygenated functional groups (OFG) were also evaluated. Results showed a consistently higher selectivity towards lactic acid (LA) across all catalysts and competitive catalytic conversion. In this performance, dopants played a crucial role in surface acid-base characteristics, while oxygenated functional groups (OFG) influenced copper adsorption, dispersion, and reducibility. Notably, the Cu/CXN-f catalyst demonstrated the highest LA yield by combining the effect of N as a doping species, with the presence of OFG and the formation of appropriated metallic Cu domains. This research underscores the potential of carbon xerogels in the tailored catalyst design, contributing to sustainable chemical production through their customizable textural and chemical properties.

1. Introduction

Environmental awareness has led humanity to prioritize sustainable fuels with minimal carbon emissions, highlighting biodiesel among these options. As a by-product of biodiesel manufacturing, glycerol is produced in significant quantities, underscoring the need to advance techniques to transform this "waste" into higher value products. Thus, the use of glycerol as a raw material has a considerable impact within the framework of the circular economy. In this sense, exists a wide range of value-added chemicals, including ethanol (Shan et al., 2022), hydrogen (Haider and Chaturvedi, 2023), 1,3-propanediol, 1,2-propanediol (Luo et al., 2023), glycerol carbonate (Jaiswal et al., 2023), glyceric acid (Yu et al., 2024; Xu et al., 2022), lactic acid (Akbulut and Özkar, 2022; Arcanjo et al., 2020), among others, which can be sourced from glycerol. These substances are usually obtained through catalysed processes, including reactions such as carboxylation, dehydration, etherification, hydrogenolysis, esterification, and oxidation, among others (Arcanjo et al., 2020; Kaloudas et al., 2021; Belousov and Suleimanov, 2021). Heterogeneous catalysts have undergone extensive scrutiny in the catalytic conversion of glycerol as they are easily separable from the resulting products. Nevertheless, certain shortcomings of heterogeneous catalysts, including inadequate thermal stability, limited regenerative capability, deactivation, reduced surface area, and the production of by-products, limit their utility. Then, the design of suitable catalysts for the conversion of glycerol into new products is an important research line, in which, factors such as the regulation of the size and shape of metallic domains, their thermal/chemical stability, their spatial distribution, their electronic configuration, and their surface composition must be considered.

Lactic acid and glyceric acid are high-value-added products obtained through the oxidation of glycerol. Lactic acid is the monomer of polylactic acid (PLA), which is considered a promising candidate as a

* Corresponding author.
** Corresponding author.
E-mail addresses: aapuente@incar.csic.es (A. Arenillas), mrmorale14@gmail.com (M.R. Morales).

https://doi.org/10.1016/j.envres.2024.119190
Received 16 April 2024; Received in revised form 17 May 2024; Accepted 20 May 2024
Available online 25 May 2024
0013-9351/© 2024 The Authors. Published by Elsevier Inc. This is an open access article under the CC BY-NC-ND license (http://creativecommons.org/licenses/by-nc-nd/4.0/).

substitute for petroleum-based plastics and is also highly sought after in the pharmaceutical and medical sectors (Taib et al., 2022; Mäki-Arvela et al., 2014; Djukic-Vukovic et al., 2019). Glyceric acid possesses biological functions and is widely utilized by pharmaceutical and food industries (Sato, 2021; Zhou et al., 2021). Numerous supports and metals have found application as catalysts in the production of these two acids. Carbonaceous supports, in particular, have gained significant prominence due to their ability to meet many of the aforementioned requirements: they offer thermal and chemical stability, facilitate physicochemical modifications of their surface through functionalization, boast high surface areas, are easily recoverable, and even allow for the retrieval of metals deposited on them via support gasification, among other advantages (Koranian et al., 2022). In the glycerol oxidation reaction, noble metals have demonstrated higher selectivity and performance towards various oxidation products, but the costs of these systems and the strong reaction conditions have led to continuing the study to reduce costs (Arcanjo et al., 2017; Demirel-Gülen et al., 2005). In this regard, transition metals like copper have achieved comparable performance through appropriate surface design, which involves controlling the distribution and size of metallic domains and fostering different types of interactions with the support (Hu et al., 2023; Zhou et al., 2011).

In our previous research (Flores-López et al., 2024), it was demonstrated that carbon xerogels serve as excellent supports for metals such as copper, and can even function as catalysts independently, without requiring the addition of metals, in the glycerol oxidation reaction. The acid-base characteristics, content and arrangement of surface oxygenated functional groups (OFG), resulting from temperature modification and/or carbonization atmosphere, combined with their textural characteristics, were responsible for the high selectivity of these supports. Due to their acidic character, the main product is glyceric acid. These surface characteristics also significantly influenced the arrangement of Cu on the surface, as well as the metal-support interaction. The catalysts obtained from these xerogels exhibited a change in selectivity, since the incorporation of Cu induced a shift in the surface's acid-base properties, rendering it more basic. This, coupled with the basic character of the reaction medium, facilitated the predominant production of lactic acid.

This work presents an extension of the aforementioned research focused on the evaluation, as supports and catalysts (with deposited Cu), of doped carbon xerogels with Si, N, and graphene oxide (GO). With the premise of the relevant role of oxygen functional groups, the doped xerogels were also functionalized, generating a second series of materials. Supports and catalysts were tested in the catalytic decomposition of glycerol and characterised to better understand their performance of these systems, particularly in terms of activity and selectivity towards reaction products.

2. Experimental

2.1. Synthesis of carbon supports

Three different carbons doped with graphene oxide (GO), nitrogen (N) and silica (Si) were used in this study. These carbons were synthesized by the sol-gel methodology, starting from Resorcinol–Formaldehyde (R, 99 % from Indspec; F, solution 37 % stabilized with 10 % of MeOH from Merck) precursor solutions to which specific compounds were added to get the desired doping. The synthesis methodology to prepare undoped carbons starts by dissolving R in distilled water under stirring. F is added with additional stirring to homogenise the mixture, and finally NaOH 1M booster is added drop by drop to adjust the required pH. The precursor mixture is heated at 85 °C under microwave radiation for 5 h to obtain the sol-gel material (Arenillas et al., 2013; Rey-Raap et al., 2014a, 2014b). For GO-doping, the distilled water used to dissolve R is replaced by an aqueous suspension of GO at 5 mg mL^{-1} from Applynano Solutions S.L., the rest of the procedure remains the same (Canal-Rodríguez et al., 2017). For N-doping, urea (99 % Acros Organics) is added and dissolved with the R and the temperature used in the sol-gel process is reduced to 70 °C (Inagaki et al., 2018). Finally, in the synthesis of the Si-doped carbon, to ensure a homogeneous co-polymerization between inorganic (SiO_2) and organic (RF) compounds, the precursor solution consists of a hydroalcoholic mixture of R, F, distilled water, ethanol (EtOH, 96 % from J.T. Baker) and tetraethylorthosilicate (TEOS, 99 % from Chem-Lab) as reported in the work (Flores-López et al., 2021). In this case, the gelation was promoted at 70 °C using conventional heating.

The amounts of each reagent used in the synthesis were calculated based on the sol-gel chemical variables shown in Table 1, designed to obtain a pore size of about 10 nm in all cases. The materials obtained were thermally treated under an inert atmosphere (N_2) at 1000 °C for 2h to carbonise the organic contribution. The GO, N and Si doped carbons obtained were labelled as CXGO, CXN and CXSi, respectively.

2.2. Functionalization of supports

Two functionalization tests were conducted on the CXSi support to determine the most effective method to introduce oxygen functional groups (OFG), which allows higher activity in the glycerol oxidation reaction (Flores-López et al., 2024). In the first method, 0.35 g of the support underwent oxidative treatment in 0.05 L of 1M HNO_3 aqueous solution at 120 °C for 3 h. Subsequently, the support was filtered, washed, and dried in an oven at 70 °C for 15 h. The second treatment involved a gas-phase procedure where 0.35 g of support was introduced into a tubular reactor inside an oven at 330 °C for 3 h under an air flow of 385 mL min^{-1}, with a heating rate of 10 °C min^{-1}. Subsequently, both treated samples were stabilized at 300 °C under a nitrogen flow for 15 h (Mager et al., 2014). The supports obtained were named CXSi-HNO_3 and CXSi-air, and both underwent testing in preliminary catalytic glycerol oxidation reactions. The support oxidized in air (CXSi-air) demonstrated the best performance in the reaction (Fig. 1 SM), so this method was selected for treating the other two supports, CXGO and CXN. Then, a total of six supports were considered for this study: CXSi, CXN, and CXGO (original supports), and CXSi-f, CXN-f and CXGO-f (functionalized supports by air treatment).

2.3. Synthesis of the catalysts

The copper precursor was deposited on the supports using the ultrasound-assisted impregnation method (Flores-López et al., 2024). An alcoholic solution (C_2H_6O-A.C.S., 99.5 %, Cicarelli) of copper nitrate trihydrate ($Cu(NO_3)_2{\cdot}3H_2O$ P.A., 99 %, Fluka) was utilized. 2 g of each xerogel were introduced into 0.015 L of the copper precursor solution to attain a 3 wt% Cu content in each catalyst. The mixture was placed in an ultrasonic bath for 1 h, pausing for 5 min every 15 min to prevent overheating and decomposition of the copper precursor. Excess solvent was removed by depositing the mixtures in a rotary evaporator at 70 °C and 40 RPM with a vacuum. The catalysts were calcined using an inert Ar atmosphere with a flow rate of 30 mL min^{-1} at 550 °C for 3 h. The catalysts were named: Cu/CXSi, Cu/CXN, Cu/CXGO, Cu/CXSi-f, Cu/CXN-f and Cu/CXGO-f.

2.4. Characterization

2.4.1. Textural properties

Textural properties were evaluated in supports and catalysts using

Table 1
Sol-gel variables used in the synthesis of the carbon supports.

Supports	R/F	D	R/Urea	R/TEOS	EtOH/TEOS	pH
CXSi	0.5	9.4*	N.A.	6	4.7	6.0
CXN	0.75	3.6	2	N.A.	N.A.	6.7
CXGO	0.5	5.7	N.A.	N.A.	N.A.	6.5

* Respect to (R + F + TEOS).

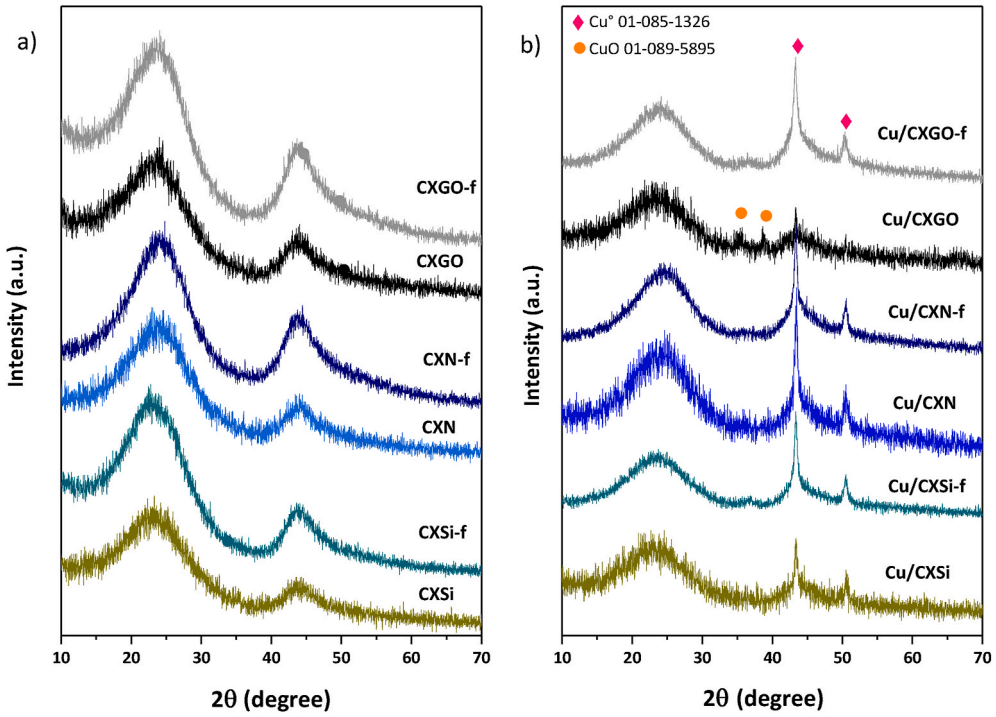


Fig. 1. XRD pattern corresponding to a) supports and b) catalysts.

helium pycnometry (AccuPyc 1330) and N_2 adsorption-desorption isotherms at −196 °C (Tristar II, Micromeritics). Before analysis, samples were outgassed under vacuum overnight at 120 °C. From helium pycnometry skeletal density (ρ_{He}) was obtained; whilst the volume of micropores (V_{micro}) was obtained by applying Dubinin-Raduskevich equation to the N_2 adsorption isotherm. Total pore volume (V_T) was evaluated at the saturation point, and mesopore volume (V_{meso}) calculated from difference between total and micropore volume. Specific surface area values were obtained by BET equation (S_{BET}), and main pore size (dp) and pore size distribution (PSD) by NLDFT, both applied to the N_2 adsorption isotherm.

2.4.2. Chemical characterization

The chemical composition (C, H, O, N wt.%) of supports was determined by elemental analysis performed with LECO-CHNS-932 and LECO-VTF-900 microanalyzers. While, in the catalyst, the Cu content was quantified using inductively coupled plasma mass spectrometry (ICP-MS, Agilent ICP-MS 7700x). Before the analysis, a digestion step was conducted with HCl: HNO_3:H_2O in a ratio of 3:2:1 for 50 min using a microwave (Milestone ETHOS-1). In addition, surface characterisation techniques were applied to elucidate the surface chemistry of supports and catalysts, paying special attention to the influence of the different doping and functionalization applied.

In supports, the functional superficial groups were determined by means of Fourier transform infrared spectroscopy (FTIR), applied to dried KBr pellets (dilution 1:500) using a ThermoNicolet-6700 FTIR spectrometer with a DTGS-KBr detector; besides temperature-programmed desorption (TPD, Micromeritics AutoChem II), performed under Ar atmosphere reaching 1000 °C using a heating rate of 5 °C min^{-1}. On the other hand, the acid-basic character of the surface was evaluated from the Point of Zero Charge pH (pH_{pzc}) determined by mass titration methodology (Žalac and Kallay, 1992), and with the isopropanol decomposition test, conducted in a stainless steel fixed-bed tubular reactor operating at atmospheric pressure, following the methodology described in previous work (Flores-López et al., 2024). A sample mass of 0.05 g (support or catalyst) was placed inside the reactor and pre-treated in Ar (150 mL min^{-1}) for 30 min at 200 °C. A total flow rate of 80 mL min^{-1} was circulated with 7.5 vol % 2-propanol in Ar at 290 °C. The reaction products were analysed using an online gas chromatograph (Buck Scientific 910) equipped with an FID detector and a silica GC column (SPB1).

In catalysts, the oxidation state of the Cu species and the presence of surface oxygenated groups, as well as the metal-support interaction were determined using X-ray Photoelectron Spectroscopy (XPS, SPECS). The acid-basic character was evaluated with the isopropanol decomposition test. The amount of reducible copper species was determined through temperature-programmed reduction (H_2-TPR) analysis. The tests were conducted using the same homemade equipment mentioned in the previous work and following the same analysis methodology (Flores-López et al., 2024). A quantity of 0.05 g of each catalyst was placed in a quartz tubular reactor, pre-treated with He (30 mL min^{-1}) at 150 °C for 30 min. After returning the samples to room temperature, a mild oxidative treatment was performed with a 20 % O_2/He mixture (35 mL min^{-1}) at 200 °C for 30 min. The reduction process was carried out using a mixture of 5 % H_2/N_2 (30 mL min^{-1}) from room temperature to 450 °C at a rate of 10 °C min^{-1}. H_2 consumptions were calibrated using reduction signals of commercial CuO (Mallinckrodt). Specific surface area, dispersion and mean particle diameter of Cu were estimated through dissociative N_2O chemisorption, using the same equipment as for H_2-TPR. The Cu dispersion and mean particle diameter were estimated using the methodology provided by Shan et al. (2020).

For structural evaluation of the present species, X-ray diffraction analysis was conducted for both, supports and catalyst, using a Rigaku Ultima IV diffractometer, which was operated at 20 mA and 30 kV and equipped with a Cu Kα ($\lambda = 0.15405$ nm) radiation source. The samples underwent scanning at a rate of 0.02° per step over the range of 10°–70°, and the resulting diffractograms were compared with the JCPDS-ICDD references.

2.5. Catalytic test

Selective oxidation of glycerol was performed in a Parr-type reactor equipped with a manometer, an oven, and temperature and stirring regulators. 20 mL of a 0.15 M aqueous solution of Glycerol (99.7 %,

Biopack), to which NaOH (≥97.0 %, Biopack) was previously added to obtain a NaOH/glycerol molar ratio = 1, was introduced into the reactor. 0.1 g of supports and catalysts were evaluated in reaction under the same conditions reported in the previous work (Flores-López et al., 2024), namely, 1 bar O_2, 90 °C, 1000 rpm and 3 h. The reaction products were identified and quantified by HPLC with external calibration of commercial standards. Conversion, product selectivity, yield, carbon balance (C.B.), turnover frequency (TOF) and Cu active sites were calculated with Equations (1)–(6):

$$GLY\ Conversion\ (\%) = \frac{moles\ of\ GLY\ converted}{moles\ of\ GLY\ in\ feed} x100 \quad (1)$$

$$Product\ Selectivity\ (\%) = \frac{moles\ of\ Products\ formed}{moles\ of\ GLY\ converted} x100 \quad (2)$$

$$Product\ Yield\ (\%) = \frac{GLY\ conversion\ (\%) x\ Product\ Selectivity\ (\%)}{100} \quad (3)$$

$$C.B.\ (\%) = \frac{moles\ C\ of\ unreacted\ GLY + moles\ C\ Pr\ oducts\ formed}{moles\ C\ of\ GLY\ in\ feed}\ x\ 100 \quad (4)$$

$$TOF\left(time^{-1}\right) = \frac{mmoles\ of\ GLY\ converted}{time\ x\ n_{Cu}} \quad (5)$$

$$n_{Cu}\ (mmoles\ of\ Cu\ active\ sites) = \frac{6\ x\ y\ x\ n_s\ x\ w_{cat.}}{d_{Cu}\ x\ \rho_{Cu}\ x\ N} \quad (6)$$

3. Results and discussion

3.1. Structural and porous properties of supports and catalyst

The crystal structure of supports and catalysts was analysed through X-ray diffraction. The XRD patterns of the supports (Fig. 1a) exhibit two broad diffraction lines at 2θ angles of approximately 26° and 42°. The first diffraction line is likely associated with the interplanar spacing of the graphite sheets in the carbon xerogel, specifically the C (002) plane (Siburian et al., 2018), while the second at a 2θ angle of 42° is a combination of peaks C (101) and C (101) (Kang et al., 2018). The low definition of such diffraction lines indicates that the supports are amorphous carbon materials without a well-defined crystallographic spacing between the graphite layers. No diffraction lines corresponding to the dopants present in the xerogels were detected. Fig. 1b shows the presence of the Cu° phase in all catalysts. The existence of this metallic species (i.e., Cu°) deposited on carbonaceous supports has been examined by several authors (Fu et al., 2017; Xiong et al., 2010), concluding that Cu undergoes self-reduction in the presence of oxygenated functional groups (OFG) on the surface of the carbonaceous supports. Thus, from the lines of Cu° detected in the XRD spectra of catalysts (Fig. 1b), it can be assumed that all the supports used in this work possess oxygen functionalities capable of interacting with the deposited Cu. Particularly, Cu/CXGO shows the lowest intensity in the Cu° diffraction lines combined with the presence of lines corresponding to the CuO phase, indicating a different interaction of the active phase and therefore different oxidation state of Cu. However, the higher intensity of the Cu° diffraction lines observed in the catalysts obtained from functionalized supports in comparison to their original counterparts, suggests the success of incorporating a higher amount of OFG in the functionalization step and its effectiveness in driving the Cu precursor into the catalyst.

Table 2 summarises the textural properties of all supports and catalysts used in this study. Starting with the support materials, the analysis of their textural characteristics can be carried out by differentiating between two series: i) the original doped-carbon supports (i.e., CXSi, CXN and CXGO) and ii) the functionalized carbon supports (i.e., CXSi-f, CXN-f and CXGO-f). The ρ_{He} of original supports is about 2 g cm^{-3}, a typical value of carbon-based sol-gel materials (Moreno et al., 2013). In comparison, the functionalized supports show a slight decrease in this property, due to the incorporation of surface functional groups, with values between 1.5 and 1.9 g cm^{-3}. More information about the porous structure of the materials is obtained from the N_2 adsorption-desorption isotherms in Fig. 2. Fig. 2a shows that all original supports present an isotherm of type IV with a hysteresis loop H1 (Thommes et al., 2015), indicating that all of them have micro and mesoporous materials without macropores in their structure. In addition to the shape of the isotherm, the materials show similar N_2 adsorbed volume at low p/p_0. This volume is attributed to defects promoted by volatilization of matter during applied carbonization, contributing approximately ~35 % of the total pore volume, which corresponds to the values of V_{micro} (c.a. 0.19 $cm^3\ g^{-1}$) and S_{BET} (~470 $m^2\ g^{-1}$) reported in Table 2. In comparison with CXN and CXGO, CXSi presents slightly higher V_{micro} and S_{BET} values due to the contribution of the silica of microporous character (Flores-López et al., 2021). The variation in the N_2 adsorbed volume at high p/p_0 is associated with differences in the pore structure promoted by the doping used. CXGO present a higher pore volume (0.6 $cm^3\ g^{-1}$) since the addition of GO does not affect the porosity designed and developed in the RF structure even after the drying or carbonization steps (Canal-Rodríguez et al., 2017), while CXN and CXSi present a slightly shrunken structure (V_T~0.5 $cm^3\ g^{-1}$) due to their lower mechanical resistance (Flores-López et al., 2021; Álvarez-Manuel et al., 2023). However, as shown by the PSD (Fig. 3) and the d_p values (Table 2), all the original supports have a similar main pore size of about 10 nm. Looking at the functionalized support series in Fig. 2, it is appreciated how the functionalization applied increase the volume of N_2 adsorbed at low p/p_0 of the isotherms, enhancing the V_{micro} (c.a. 0.22 $cm^3\ g^{-1}$) and S_{BET} (~570 $m^2\ g^{-1}$) values reported in Table 2. The formation of micropores with the functionalization applied, correlates well with the observed decrease in ρ_{He} and has been previously reported as an effect of the enlargement of defects created by the additional thermal treatments and maybe certain partial gasification (Mager et al., 2014). On their part, mesoporosity and main pore size remain the same after functionalization, keeping V_{meso} values around 0.38 $cm^3\ g^{-1}$ and d_p around 10 nm. CXSi-f isotherm shows a change in shape compared to the CXSi isotherm. This change suggests a slight modification of the porous structure related to the low mechanical resistance of the SiO_2 present in the sample, which is easily affected by the conditions used during the functionalization of CXSi (Robinson and Ross, 1970). However, the main porous parameters showed in Table 2 remains unchanged. In resume, the treatment with air (O_2) applied for functionalization results in a slightly increase in specific surface area and pore volume (mainly V_{micro}), besides a decrease in the helium density, particularly for CXN-f and

Table 2
Porous properties of the supports and catalysts studied.

Supports/ Catalysts	Density	Pore volume			Specific surface area	Pore size
	ρ_{He} g cm^{-3}	V_T $cm^3\ g^{-1}$	V_{micro} $cm^3\ g^{-1}$	V_{meso} $cm^3\ g^{-1}$	S_{BET} $m^2\ g^{-1}$	d_p nm
CXSi	2.13	0.53	0.21	0.32	533	10
CXN	2.14	0.52	0.17	0.35	415	11
CXGO	2.15	0.61	0.18	0.43	459	10
CXSi-f	1.86	0.57	0.21	0.36	533	10
CXN-f	1.51	0.57	0.20	0.36	521	11
CXGO-f	1.75	0.65	0.24	0.40	617	10
Cu/CXSi	2.16	0.43	0.15	0.28	390	11
Cu/CXN	2.14	0.62	0.17	0.44	434	12
Cu/CXGO	2.15	0.53	0.18	0.35	449	10
Cu/CXSi-f	1.86	0.56	0.20	0.36	511	10
Cu/CXN-f	1.85	0.55	0.20	0.35	502	11
Cu/CXGO-f	1.90	0.61	0.23	0.38	595	10

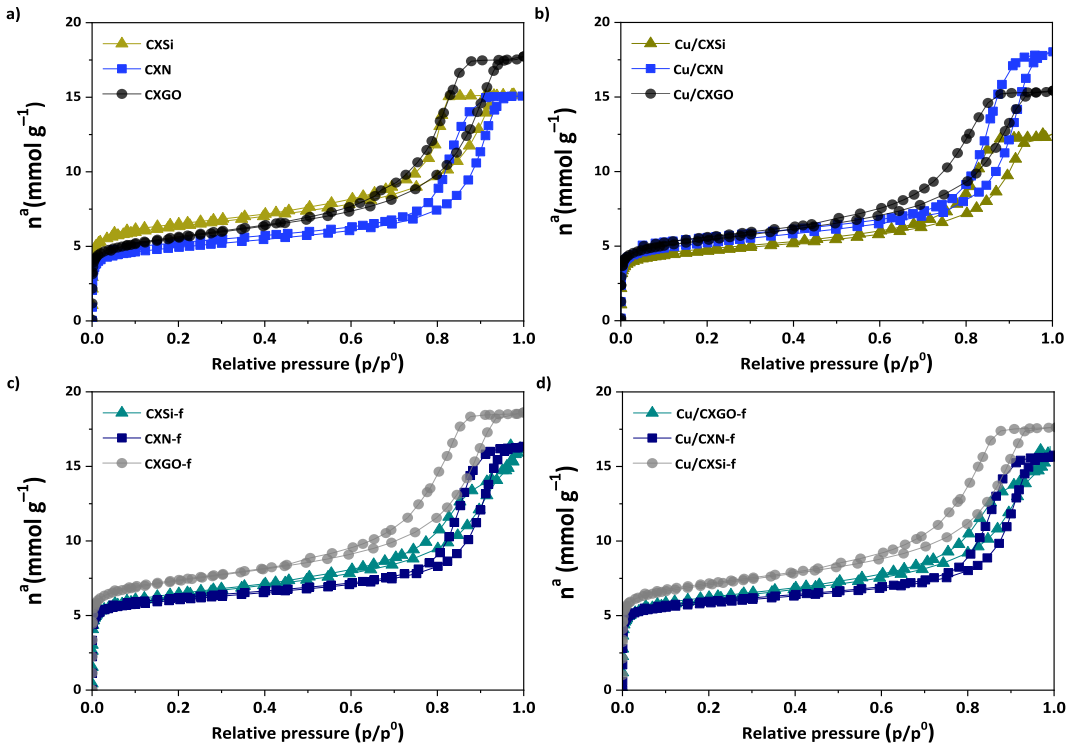


Fig. 2. N_2 adsorption-desorption isotherms of carbon-based supports and their respective catalyst. a) original supports, b) original catalyst, c) functionalized supports and d) functionalized catalyst.

CXGO-f.

The porous properties of the catalysts obtained in this study are well maintained in comparison to their corresponding supports. The isotherms in Fig. 3b show that the catalysts obtained from the original supports slightly changed their porosity. The Cu/CXSi presents a considerable reduction in microporosity (from 0.21 to 0.15 $cm^3\ g^{-1}$ of V_{micro}), which could be related to the blocking of micropores with the Cu particles. However, few literature is available on Cu impregnation of C/

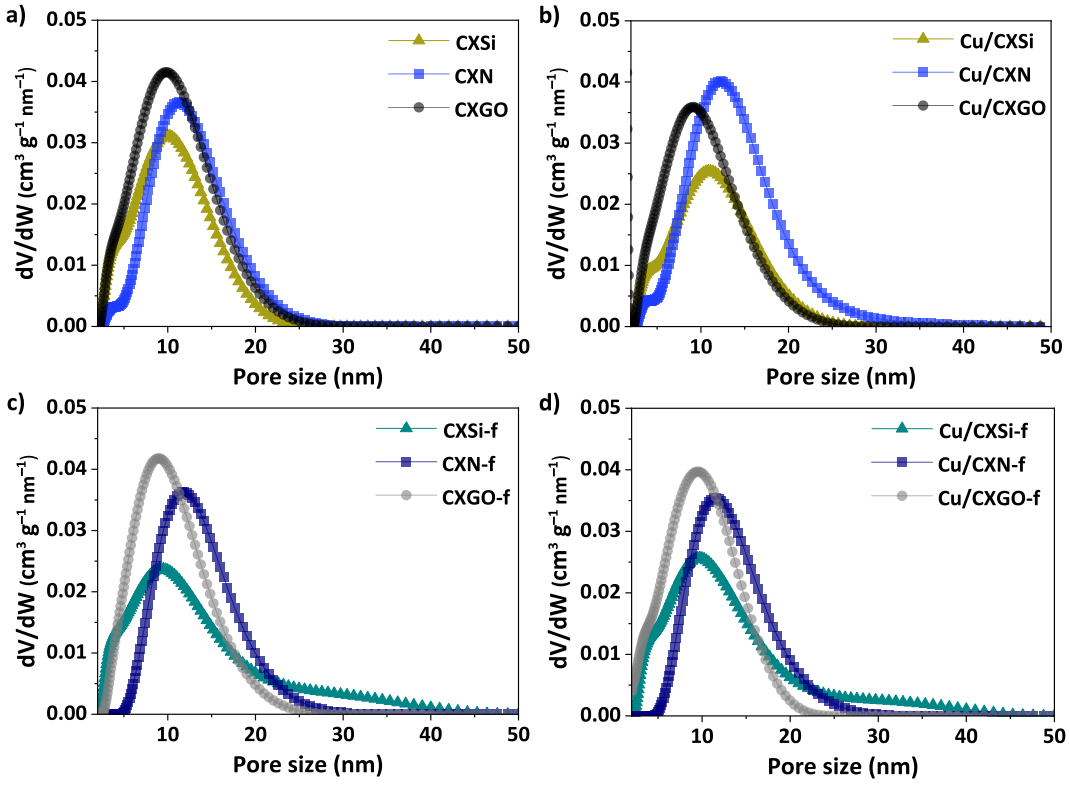


Fig. 3. Pore size distribution by NLDFT model applied to N_2 adsorption-desorption isotherms of a) original supports, b) original catalyst, c) functionalized supports and d) functionalized catalyst.

Si hybrid materials, and none of them describes the effect of the addition of metals on the porous properties of this kind of support. Cu/CXN shows an increase of mesoporosity (from 0.35 to 0.44 $m^3\ g^{-1}$ of V_{meso}) attributed to the good dispersion and configuration of Cu achieved by the improved metal-support interaction that exists when using N-doped carbons (Cheng et al., 2021). On its part, Cu/CXGO shows a decrease of mesopores (from 0.43 to 0.35 $m^3\ g^{-1}$ of V_{meso}) attributable to a reduction in the free space of these pores by the presence of Cu, a behaviour previously reported in Cu catalyst obtained from an undoped CX (Flores-López et al., 2024). These textural data already demonstrate the different mechanisms and interactions occurring by the effect of the doping species. In the catalysts obtained from functionalized supports, the porous properties are practically not affected (see Fig. 2d and 3d and Table 2). This behaviour shows the important role of the oxygenated functional groups (OFG) as the main active site for Cu coupling, avoiding the impact of Cu on the textural properties of the support (Flores-López et al., 2024; González et al., 2021).

3.2. Chemical properties of supports

In terms of chemical properties, Table 3 shows the chemical composition of the original and functionalized supports obtained by elemental analysis, with the SiO_2 content calculated based on the synthesis recipe and the ashes (Flores-López et al., 2021). The introduction of SiO_2 (10.9 wt%) and N (2.3 wt%) species in CXSi and CXN, respectively, was confirmed. With the presence of such species, the carbon content was reduced to 84 and 95.5 wt% on these samples. As expected, with the functionalization applied all the samples considerably increased their O content 2 or 3 times (see Table 3), which is in good agreement with previous reports on gaseous oxygen functionalization (Mager et al., 2014; Alegre et al., 2013). This higher oxygen content modifies the correspondent percentage of SiO_2 and N content to 7 and 1.6 wt%, respectively.

Fig. 4 shows the FTIR spectra for all the supports. CXGO shows the characteristic bands for carbon-based materials (Flores-López et al., 2024): a broad band at 1200 cm^{-1} correspondent to C–O stretching vibrations in carboxylic acids, anhydrides, lactones, ethers, and esters and bending of carboxylic acids and phenols, a band around 1600 cm^{-1} associated to C═O stretching vibration from quinones, aldehyde and carboxylic acids, small signals at 2350 cm^{-1} related to stretching vibration in ketones, bands at 2800-2900 cm^{-1} attributed to CH stretch vibration from aliphatics and a wide band at around 3400 cm^{-1} related to vibrations of hydroxyl group (-HO) in carboxyls, phenols or alcohols. With the introduction of N and Si, CXN presents differences attributed to CN stretching vibrations and NH/C═N bonds localized in bands at 1100 and 1570 cm^{-1} (Yu et al., 2014), while CXSi present a better definition in the band at 1100 cm^{-1} and new bands at 805 and 470 cm^{-1}, all of them attributed to stretching vibrations and bending modes of Si–O–Si bonds (Flores-López et al., 2021; Deshmukh et al., 2012; Chen et al., 2012). Finally, the spectra of functionalized supports CXGO-f and CXN-f show similar signals to their corresponding unfunctionalized precursors

Table 3
Chemical composition and chemistry surface of the original and functionalized supports.

Supports	Composition[a]					pH_{pzc}	CO/CO_2[b]
	C wt. %	H wt. %	O wt. %	N wt. %	SiO_2 wt. %		
CXSi	84.0	0.5	4.6	–	10.9	7.28	4.0
CXN	95.5	0.4	1.8	2.3	–	8.71	2.6
CXGO	98.1	0.4	1.5	–	–	8.72	2.4
CXSi-f	83.6	0.5	8.9	–	7.0	6.86	3.9
CXN-f	92.0	0.5	5.9	1.6	–	8.18	2.7
CXGO-f	94.3	0.5	5.2	–	–	8.17	1.6

[a] By elemental analysis.
[b] By TPD.

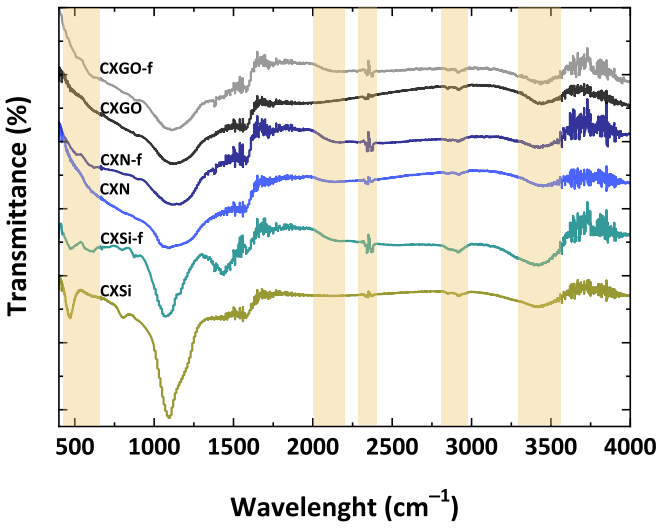


Fig. 4. FTIR spectra of carbon-based supports.

at 1200, 1600, 2900 and 3500 cm^{-1}. On its part and due to the presence of Si, CXSi-f shows a decrease in the band at 1110 cm^{-1} (corresponding to Si–O–Si groups) and an increase in –OH groups at 3500 cm^{-1}. Also, with the increment of oxygen in these functionalized supports, their spectra show the presence of additional functionalities such as ketones (an increase of band at 2900 cm^{-1}), alkyne group (new band at 2200 cm^{-1}) and C-OH (new band at 670 cm^{-1}). These functional groups have been reported when similar oxidation procedures are applied (González et al., 2021).

The surface chemistry of the supports, specifically, their acid-basic character was evaluated using the pH_{pzc} and the CO/CO_2 ratio determined by TPD. The typical value of pH_{pzc} reported for a carbon gel is around 7–8 (Figueiredo et al., 2011). Then, for the doped carbons used as supports, the pH_{pzc} values vary based on the doping applied. CXN and CXGO present a similar pH_{pzc} of 8.7 attributed to nitrogenated groups (Yang et al., 2015) and the basicity acquired by the presence of basal planes (from GO sheets) (Montes-Morán et al., 1998), respectively. For CXSi, a slight reduction in the pH_{pzc} of the carbon gels could be expected due to the acid character of silica gels (with $pH_{pzc} < 7$) (Sahai, 2002). However, CXSi reaches a pH_{pzc} similar to the carbon gels (pH_{pzc} 7.3) probably by the effect of the C/SiO_2 ratio generated in the hybrid, a tendency observed in other silica-carbon mixtures (Loureiro and Kartel, 2006). On the other hand, the functionalized supports showed a slight decrease in pH_{pzc} values due to the increase of oxygenated groups that contribute to the acidity of the surface (Ania et al., 2002). Even with this decrease, the series maintains the trend based on the applied doping (see Table 3). Fig. 5 shows in detail the CO and CO_2 profiles for both series of supports and their corresponding deconvolutions. During thermal decomposition, at low temperatures functional groups with acidic characteristics like carboxylic acids (100–400 °C), anhydrides (300–600 °C) and lactones (500–800 °C) can be found, while at higher temperatures the emission of weakly acidic phenol groups (500–800 °C) and basic carbonyl-quinones (600–1000 °C) takes place (Hotová et al., 2018). The series of the original supports present higher emissions of weakly acidic and basic groups (i.e. CO emission) with similar values of about 900 μmol CO g^{-1}. For CXN and CXGO, the emission of groups with acidic character is almost the same (c.a. 390 μmol $CO_2\ g^{-1}$), resulting in similar CO/CO_2 ratios in correspondence with their similar pH_{pzc}. However, despite having a lower pH_{pzc}, the emission of acid groups in CXSi barely reaches 225 μmol $CO_2\ g^{-1}$ (see Fig. 5), resulting in a higher CO/CO_2 ratio (c.a. 4, see Table 3). This leads to conclude that the less basic character of CXSi is not attributed to its content of acidic oxygenated groups, but to the contribution of SiO_2, which maintains an acidic character even combined in the hybrid structure. With the

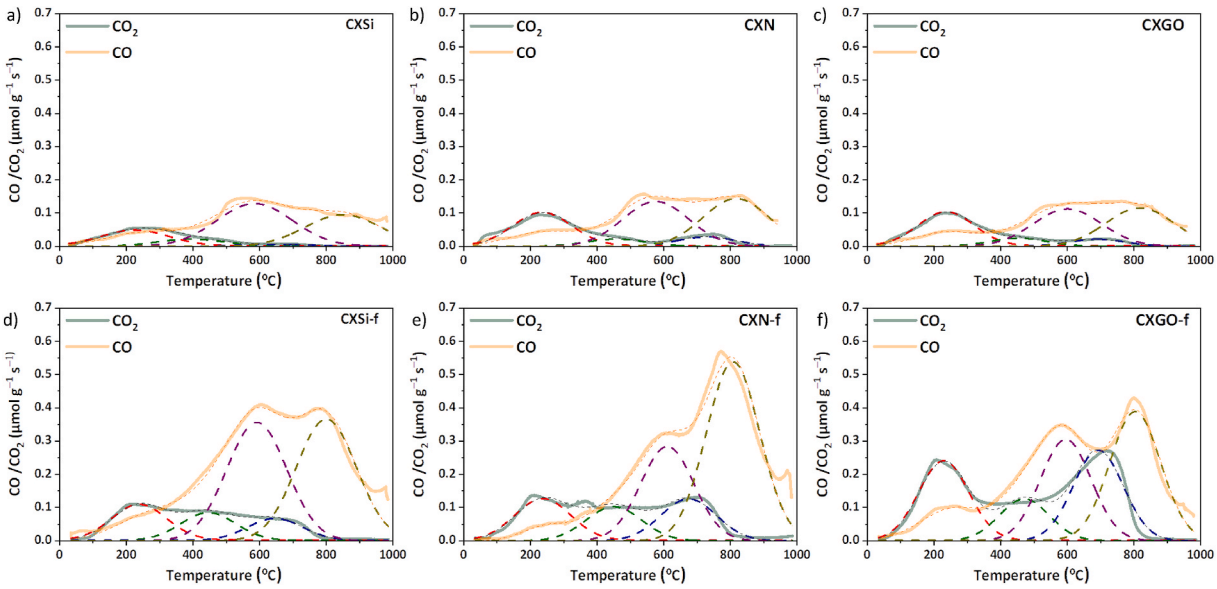


Fig. 5. CO and CO_2 TPD profiles (–) and deconvolution (— fit and individual peaks) of carbon-based supports.

increase of oxygen content in the functionalized supports, considerably higher emissions of CO and CO_2 were registered in their corresponding TPD profiles. Again, the entire series presents higher emission of weakly acidic and basic groups (i.e. CO emission), reaching values 3 times higher than the un-functionalized series (ca. 2750 μmol CO g^{-1}). As in the case of CXSi, CXSi-f has the lowest contribution of acidic oxygenated groups (ca. 650 μmol CO_2 g^{-1}) among the functionalized supports (see TPD profile in Fig. 5), while exhibiting the lowest pH_{pzc} of the series. This behaviour again shows the effect of the acid character of SiO_2, demonstrating its strong influence on the acid-base characteristics of the doped support. On the opposite, CXGO-f shows the highest content in acidic oxygenated groups (ca. 1400 μmol CO_2 g^{-1}), with a notable increase of carboxylic acids and lactones (see Fig. 5). Such an increase results in a lower CO/CO_2 ratio, which is in good agreement with the reduction of pH_{pzc} observed for CXGO-f when compared with the non-functionalized sample (i.e. CXGO). Based on the pH_{pzc} values, a similar behaviour on the CO and CO_2 profiles is expected for CXN-f. However, even if this functionalized sample has an emission of 910 μmol CO_2 g^{-1}, its CO/CO_2 ratio is higher than expected (ca. 2.7, see Table 3) due to the elevated emission of CO measured. In this case, due to the presence of N-functionalities in CXN-f, the CO profile is affected by the N_2 emission that usually appears between 600 and 1000 °C (Chernyak et al., 2019; Friedel Ortega et al., 2016). This effect is suggested by the shift and increase of the peak corresponding to quinones observed in CXN-f (Fig. 5), which causes the overestimation of the CO/CO_2 ratio for CXN-f. Although compared to other volatiles the pathways explaining the formation of N_2 are not straightforward, this product is linked to recombination of –C(N) functionalities (Friedel Ortega et al., 2016). The formation of N_2 seems to be significant only for CXN-f (not in CXN), maybe due to the instability of –C(N) bonds caused by the oxidation of the surface.

From these results, it is evident that for all supports, the surface acid-base character is governed by the functionalization applied and the presence of dopants. Functionalization with air increases both, basic and acid OFG on the surfaces (see composition in Table 3). Supports doped with N and GO (original and functionalized), predominantly basic character is observed, (see pH_{pzc} in Table 3). On their part, the Si-doped supports, despite having basic surface groups, show the lowest pH_{pzc} values associated with the acidic nature of SiO_2.

Copper contents for the two families of catalysts were determined by ICP-MS and are presented in Table 4. It can be observed that for catalysts made from original supports, the Cu content is lower, whereas for catalysts made with functionalized supports, the content matches with the theoretical added value (c.a. 3 wt%). This demonstrates that the increased capacity for Cu absorption is directly linked to the presence of surface oxygenated functional groups.

To obtain detailed information about the catalysts' surface and the superficial elemental composition, the two families of catalysts were characterized by XPS. States of carbon (C 1s), oxygen (O 1s), nitrogen (N 1s), silicon (Si 2p), and copper (Cu 2p) were analysed from the corresponding spectrum. In Fig. 6, deconvoluted C 1s spectra for all catalysts are presented showing a similar profile. From the deconvolution of these spectra, 5 common signals are observed for all catalysts, while a sixth signal (c.a. 291.0 eV) appears only for the Cu/CXGO, Cu/CXGO-f and Cu/CXN catalysts. The contribution located at a binding energy (BE) of c.a. 284.0 eV is attributed to the presence of C═C bonds, while the BE of c.a. 284.7 eV is associated with the presence of C–C bonds. The signal located at a BE of c.a. 285.4 eV has been linked to C–OH/C–O–C type bonds, while a BE of c.a. 286.4 eV is related to the C═O bond. The signals located at a BE of c.a. 288.8 eV are commonly attributed to C–C═O bonds. The sixth signal, broad and of low intensity at a BE of c.a. 291.0 eV, corresponds to the $\pi - \pi^*$ transition (Flores-López et al., 2024; Alegre et al., 2013; Segovia-Sandoval et al., 2019). Table 1 SM shows the BE and corresponding surface atomic percentages obtained from the deconvolution of the C 1s spectra of all the catalysts. In all cases, the incorporation of dopants (Si, N, and GO) induces changes in C 1s signals,

Table 4
Chemical composition by ICP-MS and XPS of the catalysis studied.

Catalysts	Cu/(Cu + C)[a] (%at.)	Cu[b] (% wt.)	d_{vs} Cu[c] (nm)	D[c] (%)	H_2 THEO [d]	H_2 EXP [d]
Cu/CXSi	1.3	2.4	4.4	23	15.1	14.8
Cu/CXN	1.8	2.5	5.8	17	15.7	15.1
Cu/CXGO	1.0	2.1	2.0	47	13.2	12.9
Cu/CXSi-f	0.4	3.0	4.0	25	18.9	8.3
Cu/CXN-f	1.3	3.0	3.2	32	18.9	6.7
Cu/CXGO-f	1.6	3.1	5.2	29	19.5	8.9

[a] Cu contents calculated based on the XPS analysis.
[b] Cu content calculated based on the ICP-MS analysis.
[c] Volume-surface diameter (d_{vs}) and dispersion (D) of Cu particles calculated by N_2O decomposition.
[d] Theoretical and experimental H_2 consumed in Temperature Programmed Reduction (H_2-TPR).

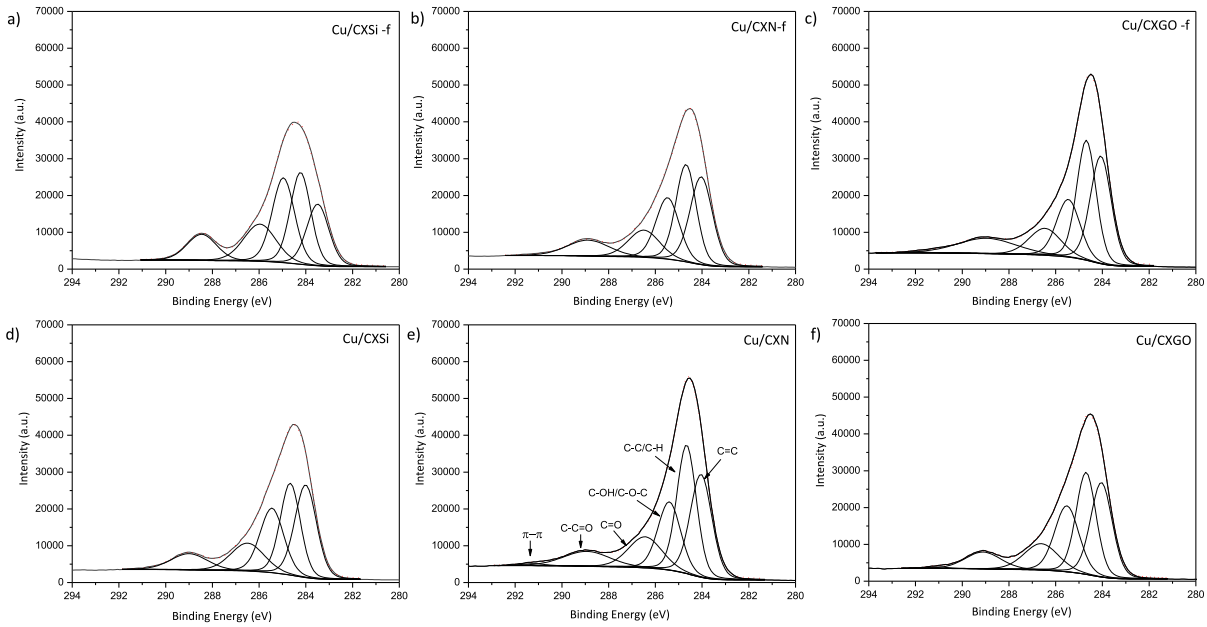


Fig. 6. Profile and deconvolution of the C 1s band from XPS spectra of original and functionalized catalysts.

shifting the BE values and modifying the distribution of surface atomic percentages from those previously reported for a catalyst obtained from an undoped support Cu/CX (Flores-López et al., 2024). The Cu/CX catalyst is taken as a reference since it was synthesized using the same synthesis method applied to the supports and catalysts under investigation in this study. Then, in comparison with Cu/CX, all the catalysts under study increase the atomic percentages of C 1s signals associated with OFG either by the effect of the dopant species or by the functionalization applied. Additionally, it can be observed that Si as doping specie eliminate the presence of $\pi - \pi^*$ transition. These results are consistent with observations from elemental analysis, TPD, and FTIR of the supports. Shifting to lower BE values is observed in all catalysts for all the C 1s states, but mainly for Cu/CXSi-f.

On the other hand, the O1s spectrum for all catalysts was deconvoluted into three signals (Fig. 7 and Table 2 SM). The signal at a BE of c.a. 530.5 eV corresponds to C═O in carbonyls and carboxylic groups. The signal with a BE of c.a. 532.2 eV is attributed to C–O–C, characteristic of phenols, lactones, ethers, and anhydride. The last signal at c.a. 533.5 eV is assigned to C(O)–OH bonds in esters and anhydride functional groups (Flores-López et al., 2024; Segovia-Sandoval et al., 2019; Morawa Eblagon et al., 2021). Comparing the O1s signals of the reference Cu/CX with the six catalysts of this study, it can be observed that the introduction of dopants only modifies the binding energies of C═O, shifting them to lower BE. This effect is more notable in catalysts from functionalized supports. The rest of the signals show no significant shifts (Table 2 SM). In terms of the distribution of the different stages of O 1s, compared with Cu/CX, C═O decreases in all cases, while increases are detected for C–O–C and C(O)–OH bonds. The tendency in the distribution percentages shows two notable values, for C(O)–OH in Cu/CXSi, and C–O–C in Cu/CXN. Both are attributable to the dopant species

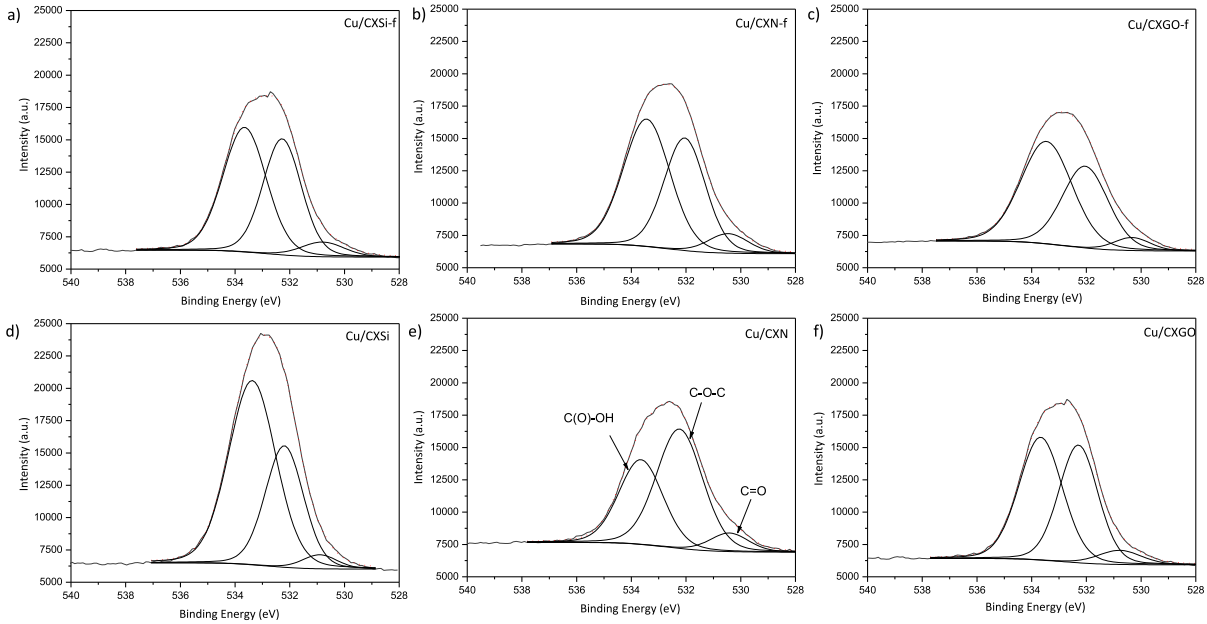


Fig. 7. Profile and deconvolution of the O 1s band from XPS spectra of original and functionalized catalysts.

present in the support. However, in the catalyst from functionalized samples, this effect is missing, since all catalysts maintain very similar percentages. The observed increase in the content of OFG-related bonds aligns with the observations made in C 1s spectra, and with the TPD and FTIR results.

Deconvoluted spectra corresponding to N 1s, for Cu/CXN-f and Cu/CXN catalysts, are shown in Fig. 8a and c. According to literature data, spectra are deconvoluted in 4 contributions. Signals at BE of c.a. 398 eV are assigned to pyridinic-N, where the N atom is located in a six-membered ring and contributes a π electron to the aromatic π system (Álvarez-Manuel et al., 2023; Yang et al., 2015; Morawa Eblagon et al., 2021; Pérez-Cadenas et al., 2009). Signals at BE 399.9 6 and 400.08 eV are attributed to pyrrolic-N and pyridone-N, but, since both groups have a similar chemical environment for the nitrogen atom (with two π electrons contributing to the π system), their assignment is not differentiated due to tautomeric equilibrium in pyridine (Pérez-Cadenas et al., 2009). Signals at BE c.a. 401.25 correspond to nitrogen atoms incorporated into a graphene layer (quaternary-N); in comparison to pyridinic-N, this is defined as nitrogen relatively more positively charged and incorporated into a graphene layer (Gorgulho et al., 2009; Boudou et al., 2003). Finally, the signal at c.a. 403.4 eV is associated with N–O bonds (Yan et al., 2004; Majumdar et al., 2012). For Cu/CXN-f, a slight shift to higher BE is observed for the four signals compared to Cu/CXN (Table 3 SM). On its part, the atomic percentages of N-species were slightly modified in the Cu/CXN-f, decreasing the pyrrolic-N and pyridone-N bonds, attributed to the higher presence of OFG and/or different interactions with Cu (Bulushev et al., 2017; Zhang et al., 2016). The surface atomic ratios of N/(N + C) are similar for both catalysts (Table 3 SM). Compared to the elemental analysis of their respective supports, this ratio is lower for Cu/CXN and similar for Cu/CXN-f (Table 3), suggesting that in the case of Cu/CXN, Cu may interact directly with N-species, which difficult their detection in the XPS technique.

The XPS spectra of Si 2p for the Cu/CXSi-f and Cu/CXSi catalysts were deconvoluted in three contributions (Fig. 8b and d and Table 3 SM). A main component corresponding to Si–O–C bonds is observed at 103.50 eV and 103.01 eV, respectively. Two signals of lower intensity are attributed to Si–C bonds (102.53 eV and 101.85 eV) and bonds associated with SiO_2 (104.30 eV and 104.08 eV) (Kaur et al., 2016). Cu/CXSi-f shows a shift to higher BE for Si–C, while Si–O–C and SiO_2 shift to lower BE (Table 3 SM). In the percentage distribution of the species, Cu/CXSi-f shows a higher content of Si–C, while the SiO_2 decreases. This suggests a promotion in the Si–C formation by the effect of the OFG formed during functionalization. It is noticeable that the surface atomic ratio Si/(Si + C) for both catalysts are lower than that reported by elemental analysis (Table 3), which means that just a small quantity of Si is exposed on the surface of the catalysts.

In Fig. 9, deconvoluted Cu 2p spectra for all catalysts are presented. In all spectra, the presence of a satellite signal at approximately 943 eV is observed, characteristic of CuO, associated with the d9 configuration of Cu^{2+} (Yuan et al., 2018). The signals corresponding to Cu 2p3/2 and Cu 2p1/2 were deconvoluted into 2 signals corresponding to Cu^{2+} at ≈ 953.6 eV–934.6 eV and Cu^{+}/Cu° at ≈952.5 eV–932.6 eV. Even if the BE of Cu^{+}/Cu° is not easily distinguishable in the Cu 2p3/2 signal, for deconvolution it was considered the XRD result, where the presence of Cu° is clearly observed in all catalysts (Sarkodie et al., 2021; Wu et al., 2006). Among the catalysts from original supports (Fig. 9) Cu/CXN shows a higher intensity of Cu signals, suggesting a higher content of superficial Cu. Also, the highest shift to lower BE for Cu^{+}/Cu is found in Cu/CXN. Even if this behaviour could mean a poor interaction with Cu in comparison with the rest of the supports, it has been demonstrated that strong metal-support interaction is promoted in N-doped samples due to the higher availability of unpaired electrons in N, which promotes the adsorption of Cu during the impregnation (Yang et al., 2015; Bulushev et al., 2017; Zhang et al., 2016). Cu/CXSi and Cu/CXGO present higher BE corresponding to Cu 2p than Cu/CXN, indicating a

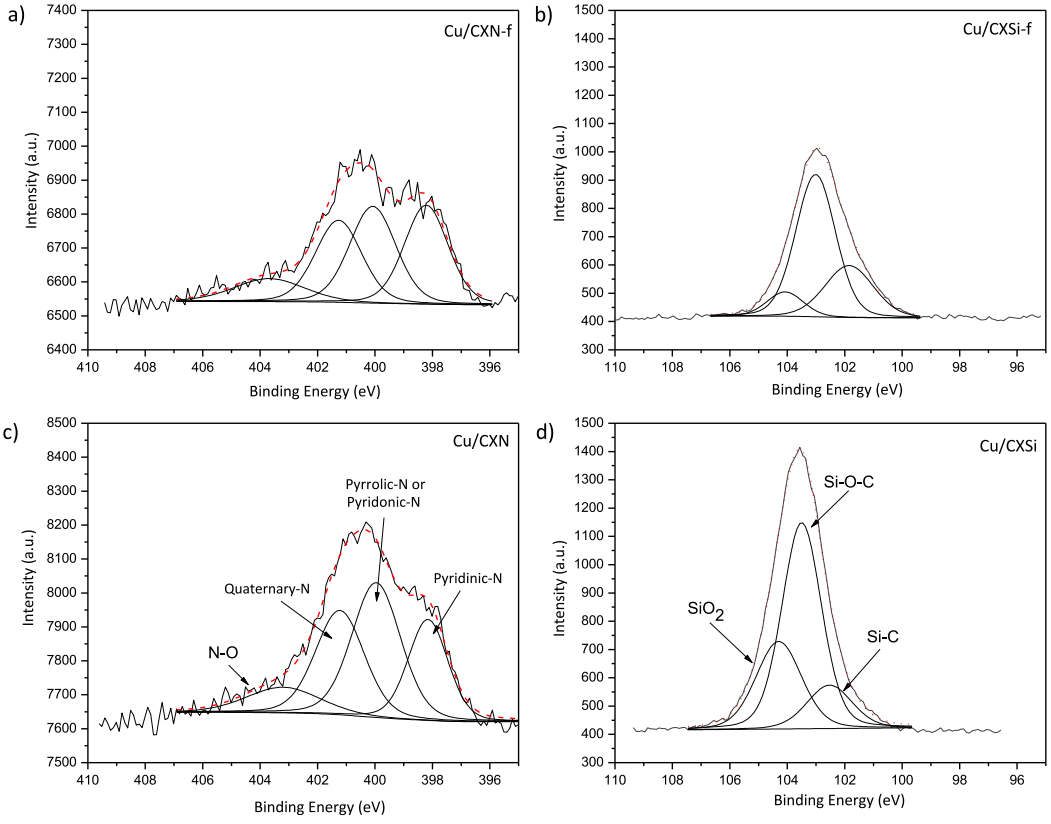


Fig. 8. Profile and deconvolution of the N 1s and Si 2p bands from XPS spectra of original and functionalized catalysts.

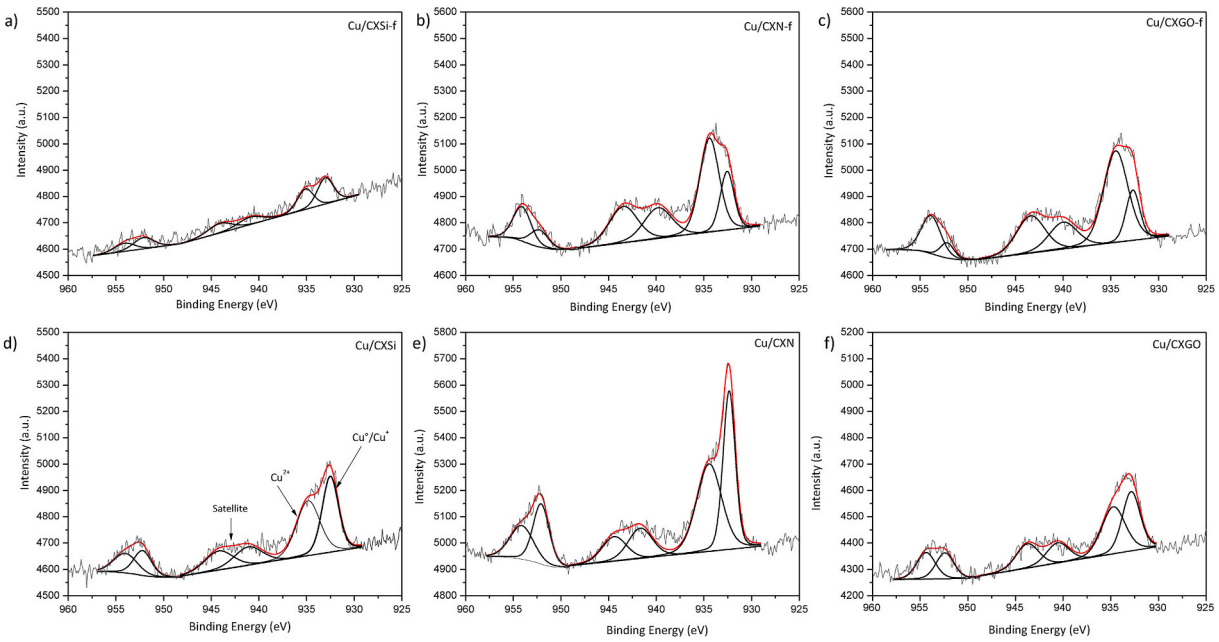


Fig. 9. Profile and deconvolution of the Cu 2p band from XPS spectra of original and functionalized catalysts.

different metal-support interaction for these catalysts. Then, the higher BE values corresponding to C 1s and O 1s could indicate a slightly greater interaction for Cu/CXGO. The surface atomic copper contents for the three catalysts are lower than those obtained from ICP-MS (Table 4), indicating that part of the Cu could be located at pore depths greater than 4 nm, which is approximately the photoelectron escape depth for XPS (Fuentes-Perujo et al., 2006). Despite the active role of OFG in the Cu deposition, all catalysts from functionalized supports showed lower Cu percentages in XPS when compared with the ICP-MS results (see Table 4). This means that most of Cu is not located superficially. Cu/CXSi-f shows the Cu peaks with the lowest intensity (Fig. 9). As mentioned earlier, this catalyst has a slightly contracted structure due to the presence of silica, which could explain the lower superficial Cu content. Additionally, the BE of Cu/CXSi-f is shifted to lower values in C 1s, Si 2p and Cu 2p, and shifted to higher values in O 1s, this could suggest a metal-support interaction mainly promoted by the OFG present in the catalyst. On the opposite, Cu/CXGO-f has the highest pore volume (V_T) and specific surface area (S_{BET}), so a larger quantity of Cu could be incorporated on the surface, increasing its detection. In addition, its BE shifts for C 1s, Cu 2p and O 1s in the opposite directions than for Cu/CXSi-f, indicating a weaker interaction of Cu with the acid OFG found in this support (i.e., CXGO-f). In an intermediate position, Cu/CXN-f shows a surface atomic Cu content of 1.3 % and BE values closer to those of the Cu/CXGO-f catalyst, but N 1s signals shifted to higher BE compared to the Cu/CXN catalyst (Table 3 SM), indicates a different metal-support interaction.

From the analysis of the XPS results, it can be observed that the surface distribution of Cu and the metal-support interaction depends on

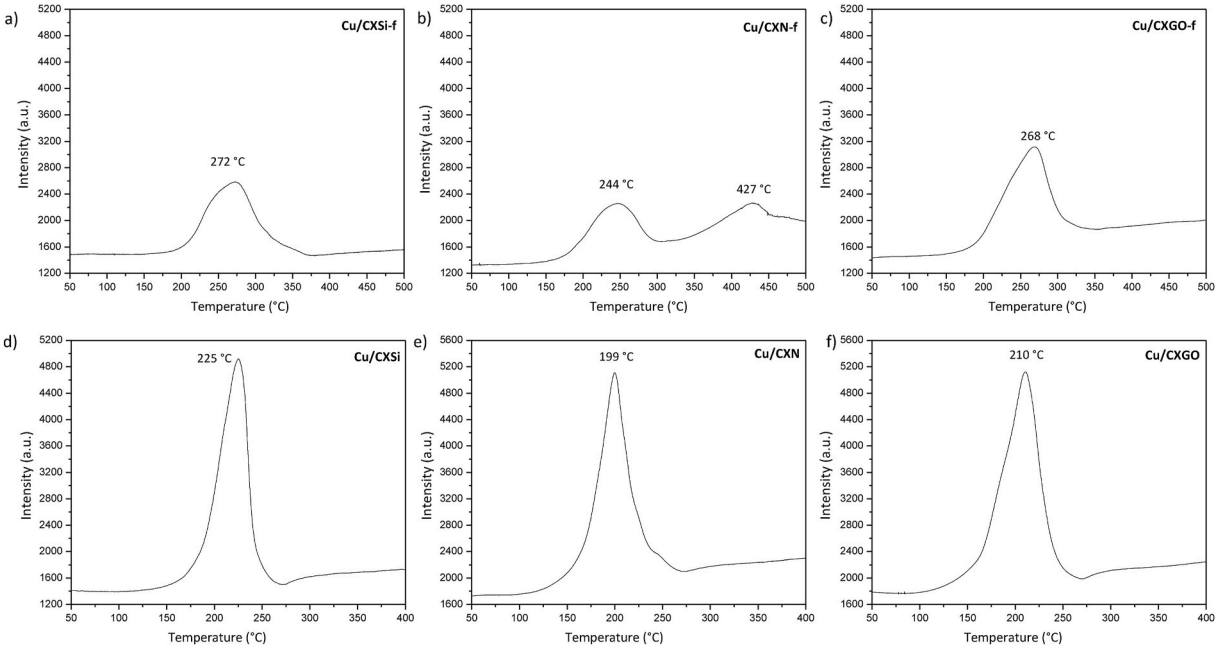


Fig. 10. H_2-TPR patterns of catalysts.

the textural properties of the supports but particularly on their surface chemistry.

The profiles of H_2-TPR for the catalysts are presented in Fig. 10. As a reference, the two families of supports were also subjected to H_2-TPR, but no reduction signals were registered within the range of temperature applied. On their part, catalysts from original supports showed a single intense reduction signal associated with the exclusive reduction of Cu. The reducibility of the catalysts follows the order: Cu/CXN > Cu/CXGO > Cu/CXSi. This order is in good agreement with the BE of Cu^{2+} reported in Table 4 SM. For these catalysts, the reduction temperatures of copper oxide are notably lower than that reported for bulk CuO (c.a. 320 °C). These low values may be associated with high dispersion and/or small domain sizes of the Cu, coupled with the different metal-support interactions. The theoretical and experimental H_2 consumptions presented in Table 4, showed that in catalysts from original supports, Cu is mainly present in the oxidized form (CuO) and to a lesser extent Cu°. For the catalysts whose supports were functionalized, the reduction profiles changed significantly, with signals of lower intensity and broader (Fig. 10). Cu/CXN-f profile shows a second signal of very low intensity at a high temperature, indicating the presence of two types of CuO species. The signal at a high temperature can be attributed to Cu species with strong interaction with the support, specifically with nitrogen species (such as N-pyridinic and/or N-graphitic). Belushev et al. (Bulushev et al., 2017) reported that Cu species stabilize in pyridinic N-species. They identified individual Cu atoms in N-doped catalysts and attributed their presence to the strong coordination between Cu and pyridinic nitrogen atoms at the edge of the graphene sheets of the support. Other authors found a preferential and strong interaction of Cu species with graphitic N-species, since the presence of unpaired electron pairs can facilitate metal absorption (Yang et al., 2015; Zhang et al., 2016). These findings are in good agreement with the increment of N-pyridinic species reported for Cu/CXN-f. For the primary reduction peak, the reducibility of these catalysts followed the same order as that of catalysts from original supports. In this regard, higher BE values (see Table 4 SM) demonstrate the higher stability of Cu in Cu/CXGO-f, while for Cu/CXSi-f, the difficult reduction could be related to the low availability of Cu on the surface coupled to the presence of OFG with very low stability (see Table 1 SM). The reduction temperatures in catalysts from functionalized supports are higher than those observed in catalysts from original supports, suggesting that the surface OFG incorporated through functionalization generates a stronger support-metal interaction. The H_2 consumption values (Table 4) highlight the self-reduction of Cu because of the OFG incorporated into the support during functionalization. It can be observed that, for all three catalysts, the experimental consumptions are less than 50 % of the theoretical values. Cu/CXN-f shows the lowest consumption, indicating a higher content of Cu° which matches with the XRD profile of the catalyst (see Fig. 1).

Before programmed thermal reduction, both families of catalysts underwent a moderate treatment for oxidizing almost all the copper. This had a greater influence on the copper domains in the original supports. In contrast, in the catalysts with functionalized supports the higher achieved metal-support interaction led to partial oxidation of the Cu domains, as clearly seen in the H_2 consumptions reported in Table 4.

The copper metal domain size (d_{vs}) was determined in all catalysts through dissociative N_2O chemisorption (Table 4). In the series of catalysts from original supports, Cu/CXN and Cu/CXSi, which exhibit the highest superficial Cu contents, show the largest d_{vs}. Conversely, Cu/CXGO, with the lowest Cu surface content and the highest S_{BET}, exhibits the smallest d_{vs}. In the group of catalysts from functionalized supports, is Cu/CXGO-f which has the highest superficial Cu content and the highest d_{vs} (5.2 nm); although Cu/CXSi-f has the lowest superficial Cu content, it forms domains of appreciable sizes (4.0 nm); and Cu/CXN-f presents the smallest Cu d_{vs} (3.2 nm).

For the catalysts containing Si in their supports, despite having completely different Cu surface contents, their d_{vs} values are similar and of moderate dispersion (c.a. 24 %). It has been reported that CuO achieves good dispersion on SiO_2 supports (Gervasini et al., 2006). Then, if for such catalysts a relationship is established between the superficial Cu content (Table 4) and the surface atomic percentage of SiO_2 obtained from XPS (Table 3 SM), their similarity could indicate that Cu is preferentially located on the superficial SiO_2. In the case of catalysts containing N in their supports, the functionalization process was crucial for favouring a decrease in d_{vs} and a better dispersion of Cu. Based on the findings of Yang et al. (2015) and Bulushev et al. (2017), the particular and strong metal-support interaction of Cu/CXN-f could be associated primarily with the presence of N-pyridinic groups. Contrary to this observation, in the catalysts with GO incorporated into the support, the functionalization promotes an increase in d_{vs} and poor dispersion. This could be associated with the higher surface content of acidic-character OFG (Table 3) and/or the -HO^- groups located on the basal planes of the superficial GO (Montes-Morán et al., 1998), which could limit the dispersion of Cu.

3.3. Catalytic test

Table 5 presents the results of catalytic activity in the glycerol oxidation reaction for supports and catalysts. Since Cu° was detected in all catalysts, they were evaluated without prior reduction, potentially allowing the omission of a step, and positively impacting the future scalability of the process. In both, supports and catalysts, the identified reaction products were oxalic acid (OA), formic acid (FA), lactic acid (LA), and glyceric acid (GA), showing a higher selectivity towards LA in all cases, and a lesser extent towards GA. According to the scheme presented in a previous work (Flores-López et al., 2024), the production of LA is favoured by the presence of surface sites with basic character (OFG, dopants and metals) and the base (NaOH) added to the reaction medium (Razali and Abdullah, 2017; Lakshmanan et al., 2013). The production of GA, on the other hand, is enhanced by a surface with a more acid character (Villa et al., 2015). Since basic and acid sites coexist in supports and catalysts, the production of both products is expected. Furthermore, based on the chemical differences that the supports and catalysts in this study have shown compared to the undoped CX and Cu/CX references, a different product distribution is to be expected.

The original supports exhibited a higher conversion of GLY than the functionalized supports, with Si-doped supports being the most active. The high conversion showed by Si-doped supports, could be associated with a favourable effect of the SiO_2 since S_{BET} is the same for both samples and the conversion value is almost not affected by the functionalization applied. On their part, CXN-f and CXGO-f present a notable drop in conversion values. As shown in Table 2, functionalization results in heightened microporosity for both supports, potentially impeding GLY absorption due to its relatively large size (c.a. 0.62 nm), thereby limiting its penetration into the micropores and consequently reducing

Table 5
Conversion, selectivity to oxalic (OA), glyceric (GA), lactic (LA) and lactic (LA) acids, carbon balance (C.B.) and turnover frequency (TOF) for supports and catalysts in the GLY oxidation reaction.

Supports/ Catalysts	Conversion % (mol)	Selectivity % (mol)				C.B. (%)	TOF (h^{-1})
		OA	GA	LA	FA		
CXSi	18.9	0.08	4.3	8.5	2.6	84	–
CXN	15.7	0.06	4.8	10.9	3.1	87	–
CXGO	10.6	0.09	7.0	16.4	5.3	93	–
CXSi-f	21.4	0.02	3.3	40.9	9.1	90	–
CXN-f	6.4	0.16	10.5	34.5	28.0	100	–
CXGO-f	4.5	0.33	20.0	60.6	18.8	100	–
Cu/CXSi	20.5	3.17	30.2	52.8	10.2	99	0.066
Cu/CXN	20.8	1.06	27.1	54.4	17.3	100	0.140
Cu/CXGO	11.6	0.54	28.4	55.2	15.8	100	0.012
Cu/CXSi-f	33.4	1.67	19.7	39.3	30.4	97	0.100
Cu/CXN-f	37.4	4.05	18.8	41.5	16.7	97	0.066
Cu/CXGO-f	28.6	0.92	22.6	52.0	15.2	93	0.202

their activity. However, the functionalized supports showed higher selectivity (particularly for LA) and C.B. of about 99 % because of OFG incorporation. In our previous study (Flores-López et al., 2024), undoped xerogel supports treated at different temperatures were evaluated in the same reaction and under the same conditions. These supports showed high activity in GLY oxidation and were particularly selective to GA production, a behaviour directly related to the presence of OFG of an acidic nature. Conversely, the selectivity towards reaction products is different when the carbon xerogel is modified. The selectivity towards LA for all the supports evaluated in this study is directly associated with the basic surface character of the supports (see pH_{pzc}), linked to the incorporated dopants and the basic OFG detected in both, original and functionalized supports (see TPD and FTIR results). The presence of acidic OFG in original supports, and their notable presence in CXGO-f, favours the selectivity towards GA, following that of LA. However, for CXSi-f and CXN-f, the elevated content of basic OFG introduced through functionalization, is likely accountable for the selectivity towards LA.

As reported in our previous work (Flores-López et al., 2024), the incorporation of Cu increases the surface basic character of the catalysts, favouring the selectivity towards LA, and to a lesser extent to GA. The same tendency is observed in the catalysts from doped xerogels (original and functionalized) evaluated in this study (see Table 5), where higher selectivity corresponds to LA and followed by GA. As in the catalytic evaluation of supports, FA has been detected, but its selectivity has particularly increased in the catalysts. It has been reported that the decomposition of GA and C–C cleavage produces acetic acid and formic acid (FA) when glycerol oxidation is carried out under oxygen pressure and basic conditions (Deng et al., 2015). Then, the FA could derive directly from the decomposition of GA, favoured by the presence of Cu and the basic OFG incorporated through the functionalization (most notably for Cu/CXSi-f).

Regardless of the behaviour shown by each catalyst, all of them show notable selectivity values compared with their supports, which is attributed almost exclusively to the presence of Cu. On the other hand, also compared to the supports, the GLY conversion values increase when catalysts are used. In the catalysts whose supports were functionalized, the increases in conversion are notably higher. Moreover, independently of the used support (i.e., original or functionalized), the catalytic activity decreases based on the doping species following the order: Cu/CXN, Cu/CXN-f > Cu/CXSi, Cu/CXSi-f > Cu/CXGO, Cu/CXGO-f.

The rotation frequency (TOF) was calculated for all catalysts (Table 5) to determine the quality of the active metal sites, since as can be seen, the supports also contribute to the oxidation reaction. Cu/CXN, which exhibits the highest TOF value and conversion among the catalysts form the pristine supports, has the highest superficial Cu content (1.8 % Cu), larger average crystallite size (d_{vs} 5.8 nm), and low interaction with the support (based on BE of the different species and its T_{red} of 199 °C). Cu/CXSi shows an intermediate TOF and conversion, related to its superficial Cu content of 1.3 %, a d_{vs} of 4.4 nm, and the greater interaction with the support (associated with the preferential location of Cu on SiO_2 and its T_{red} of 225 °C). On its part, Cu/CXGO with the smallest average crystallite size (2.0 nm) and an intermediary T_{red} (210 °C), shows the lowest conversion and TOF, attributed to the lowest superficial Cu content (1.0 %) and the presence of the CuO phase identified by XRD. From these results, it can be inferred that the catalytic behaviour of these catalysts is directly related to the metal content and its interaction with the support.

Within the family of catalysts from functionalized supports, Cu/CXN-f exhibits the highest conversion but the lowest TOF (Table 5), while Cu/CXGO-f has the lowest conversion and the highest TOF. The lowest TOF of Cu/CXN-f could be associated with its smaller d_{vs} (3.2 nm), however, its higher conversion is favoured because the incorporated OFG promote a strong metal-support interaction (observed in XPS and H_2-TPR results) useful for the oxidation of GLY. Similarly, the highest TOF corresponding to Cu/CXGO-f is attributed to its high d_{vs} (5.2 nm), but in terms of its conversion, the value is influenced by a combination of good dispersion and the presence of Cu°, resultant from the metal-support interaction occurring the material. On its part, Cu/CXSi-f presents an intermediate TOF and a d_{vs} of 4.0 nm, related to an intermediary conversion value (i.e., 33 %). However, the low availability of superficial Cu in this sample (just 0.4 %) reduces their selectivity to LA, giving a distribution of reaction products more influenced by the OFG than for Cu.

According to the calculated TOF values, larger Cu metallic domains are more efficient in the oxidation of GLY (Cu/CXN and Cu/CXGO-f). However, original and incorporated OFG, as well as the functional groups corresponding to the dopants, highly influence the interaction of the metallic phase with the surface, having a direct effect on the catalytic performance.

Reuse cycles in the catalytic reaction were carried out using the catalysts Cu/CXN-f and Cu/CXSi-f, as well as their respective supports (CXN-f and CXSi-f), which exhibited the highest and lowest LA yields (calculated from conversion and LA selectivity percentages), respectively. The results from the reuse cycles are presented in Table 6. When the supports are used, the conversion percentages decrease with each reuse, evidencing the deactivation of the materials by more than 50 % after 2 cycles. In terms of selectivity, different behaviours are registered for each support. For CXSi-f, with reuse cycles, there is a decrease in selectivity towards LA and an increase in selectivity towards GA, indicating an increase in the surface acidity of the support, either due to the reduction of basic OFG and/or greater surface exposure of Si, which has an acidic character. For CXN-f support the opposite occurs; with reuse cycles, there is an increase in selectivity towards LA and to a lesser extent towards GA. This could be due to increased surface exposure of the basic N functional groups after the loss of the incorporated and more labile OFG. In general, the reuse of functionalized supports leads to the loss of labile OFG that decreases the activity and exposes functionalities associated with dopants, thus altering their surface acid-base character according to the acid-base nature of each dopant and consequently, the distribution of the reaction products.

In the case of the reuse of catalysts, considerable deactivation is also observed (Table 6), but the selectivity towards LA and GA increases in both cases. As in the case of supports, the decrease in conversion could be associated with the loss of labile OFG, but also the loss of Cu, leaving surface characteristics similar to those of catalysts from unfunctionalized support, which enhances the formation of LA and GA. The difference in conversion percentage and the similar product distribution between the second recycles of CXN-f and Cu/CXN-f, indicates that the conversion of GLY has a direct relationship with the metal, while the selectivity towards different reaction products is associated with surface acid-base characteristics; which in the case of carbonaceous supports depend on the present OFG and/or incorporated dopants.

Table 6
Conversion, selectivity, carbon balance, and LA yield for supports and catalysts, fresh and after reuse cycles.

Supports/ Catalysts	Conversion % (mol)	Selectivity % (mol)				C.B. (%)	LA Yield (%)
		OA	GA	LA	FA		
CXSi-f	21.4	0.02	3.3	40.9	9.1	90	8.7
R1 CXSi-f	8.1	0.20	22.2	30.2	10.7	97	2.4
R2 CXSi-f	5.6	0.10	11.7	34.5	10.5	97	1.4
CXN-f	6.4	0.16	10.5	34.5	28.0	100	2.1
R1 CXN-f	4.2	0.17	13.5	38.2	12.8	97	1.6
R2 CXN-f	2.9	0.26	19.1	48.1	16.2	98	1.4
Cu/CXSi-f	33.4	1.67	19.7	39.3	30.4	97	13.2
R1 Cu/CXSi-f	13.3	0.18	32.5	46.7	13.9	99	6.2
R2 Cu/CXSi-f	9.6	0.17	28.5	47.1	9.6	100	4.5
Cu/CXN-f	37.4	4.05	18.8	41.5	16.7	97	15.5
R1 Cu/CXN-f	19.5	0.42	29.9	51.1	19.5	99	10.0
R2 Cu/CXN-f	12.6	0.09	29.2	48.8	12.6	99	6.1

Post-reuse cycle characterization of supports and catalysts was also conducted. The fresh and reused supports were characterized using a 2-propanol decomposition test (see Table 5 SM). This test allows to study the surface acid-base properties of catalytic solids based on the products obtained from the decomposition reaction (Fuentes-Perujo et al., 2006; Gervasini and Auroux, 1991; Rinaudo et al., 2022). The obtention of propylene and/or isopropyl ether means that the surface presents acidic sites, while the generation of acetone is related to basic, acid-base, and redox centres (Fuentes-Perujo et al., 2006; Chen et al., 2001). As shown in Table 5 SM, for both supports, there is a decrease in conversion, indicating a decrease in the number of total sites. For CXSi-f, a decrease in both acidic and basic sites is observed, with the acidic sites always being more abundant. This supports the previous inference regarding a greater surface exposure of Si (acidic character) due to the loss of OFG. For CXN-f, a decrease in acidic sites and an increase in basic sites are observed, consistent with the proposal aforementioned, a higher surface exposure of N-groups (basic character) due to the loss of labile OFG.

The catalysts after reuse cycles were characterized by XRD (Fig. 2 SM) and H_2-TPR (Fig. 3 SM). Both techniques reveal the leaching of Cu. XRD for the reused catalysts does not show diffraction lines of phases containing Cu (Cu° and/or CuO). The absence of Cu° is expected since no prior reduction of the catalyst was performed before each reuse cycle; however, signals corresponding to CuO could be expected due to the oxidizing reaction atmosphere, but the copper content should be so low that it is likely below the detection limit of the technique. H_2-TPR, on the other hand, effectively shows the presence of CuO in both catalysts but at much lower levels than those present in fresh catalysts, confirming the leaching of the metal; with a lower loss in Cu/CXN-f. The higher reduction temperature showed in the TPR of this catalyst demonstrates that only CuO with strong interaction with the support remains after cycling.

Comparing the catalytic behaviour of the supports and catalysts from the previous work with those studied in this research, it is appreciated that in the particular case of doped xerogels, the selectivity towards reaction products is directed by the acid-base nature of each dopant, with LA being more selective in this case; while for undoped xerogels, it depends on the surface OFG, making these materials more selective towards the production of GA. However, the lower activity of the doped xerogels compared to undoped xerogels may be due to the loss of OFG in the carbonization stage. Moreover, the OFG incorporated with gas-phase functionalization are not sufficient to reach the conversion levels reported for undoped xerogels. In both cases, the incorporation of Cu has the same effect: an increase in surface basic character, resulting in higher selectivity towards LA and, to a lesser extent, towards GA. However, catalysts from doped xerogels exhibit greater stability over reuse cycles, which may be due to the increased interaction of the metal with the functional groups associated with the doping species. It is worth noting that carbon xerogels with or without dopants are attractive materials that can act as catalysts themselves, without the need for the addition of metals, controlling their catalytic performance and selectivity by the use of simple treatments (as functionalization or doping).

4. Conclusions

Doped xerogels (Si, N, or GO), both original and oxygen functionalized, were employed as catalyst supports containing Cu as the metal. Supports and catalysts were evaluated in the glycerol oxidation, demonstrating in all cases a higher selectivity towards LA and, to a lesser extent, GA. The selectivity towards LA is associated with the surface basic character of the supports, which increase in the catalysts with the incorporation of Cu. The dopants play a decisive role in the surface acid-base characteristics, while the OFG govern the adsorption of copper, affecting its dispersion, metallic domain size, oxidation state, and consequently reducibility through different metal-support interactions. Catalysts with larger metallic domain sizes, Cu/CXN and Cu/CXGO-f, showed the highest TOF. The highest LA yield was achieved with the Cu/CXN-f catalyst, attributed to the presence of N groups, which provide basicity to the surface, enhance Cu adsorption, and improve the metal-support interaction, increasing the content of Cu°.

In addition to acting as excellent supports for metallic phases, carbon xerogels are versatile materials that allow for extensive modification of their textural and chemical characteristics, making them easily adaptable materials to act as catalysts themselves in numerous catalytic reactions with varying requirements.

CRediT authorship contribution statement

Naila Gómez González: Writing – original draft, Methodology, Investigation, Formal analysis. **Samantha L. Flores-López:** Writing – original draft, Investigation, Formal analysis. **Luis E. Cadus:** Validation, Supervision, Resources. **Ana Arenillas:** Writing – review & editing, Supervision, Resources, Project administration, Conceptualization. **María R. Morales:** Writing – review & editing, Supervision, Resources, Project administration, Investigation, Conceptualization.

Declaration of competing interest

The authors declare the following financial interests/personal relationships which may be considered as potential competing interests: Ana Arenillas reports financial support was provided by Spain Ministry of Science and Innovation. Samantha L. Flores reports financial support was provided by Government of Principality of Asturias. Maria R. Morales reports financial support was provided by National Agency for the Promotion of Research Technological Development and Innovation. If there are other authors, they declare that they have no known competing financial interests or personal relationships that could have appeared to influence the work reported in this paper.

Data availability

Data will be made available on request.

Acknowledgements

Authors gratefully acknowledge the founding received through PID2020-113001RB-I00 MCIN/AEI-10.13039/501100011033 projects granted by Ministerio de Ciencia e Innovación from Spain and European Union NextGeneration EU/PRTR; and Principado de Asturias, Spain, SLFL grant through “Severo Ochoa” program. The authors are also grateful to the Universidad Nacional de San Luis (UNSL), Agencia Nacional de Promoción Científica y Tecnológica (ANPCyT) and Consejo Nacional de Investigaciones Científicas y Técnicas (CONICET) for their financial support.

Appendix A. Supplementary data

Supplementary data to this article can be found online at https://doi.org/10.1016/j.envres.2024.119190.

References

Akbulut, D., Özkar, S., 2022. A review of the catalytic conversion of glycerol to lactic acid in the presence of aqueous base. RSC Adv. 12, 18864–18883. https://doi.org/10.1039/D2RA03085C.

Alegre, C., Gálvez, M.E., Baquedano, E., Moliner, R., Pastor, E., Lázaro, M.J., 2013. Oxygen-functionalized highly mesoporous carbon xerogel based catalysts for direct methanol fuel cell anodes. J. Phys. Chem. C 117, 13045–13058. https://doi.org/10.1021/jp400824n.

Álvarez-Manuel, L., Alegre, C., Sebastián, D., Eizaguerri, A., Napal, P.F., Lázaro, M.J., 2023. N-doped carbon xerogels from urea-resorcinol-formaldehyde as carbon matrix for Fe-N-C catalysts for oxygen reduction in fuel cells. Catal. Today 418, 114067. https://doi.org/10.1016/j.cattod.2023.114067.

Ania, C.O., Parra, J.B., Pis, J.J., 2002. Influence of oxygen-containing functional groups on active carbon adsorption of selected organic compounds. Fuel Process. Technol. 79, 265–271. https://doi.org/10.1016/S0378-3820(02)00184-4.

Arcanjo, M.R.A., Silva, I.J., Rodríguez-Castellón, E., Infantes-Molina, A., Vieira, R.S., 2017. Conversion of glycerol into lactic acid using Pd or Pt supported on carbon as catalyst. Catal. Today 279, 317–326. https://doi.org/10.1016/j.cattod.2016.02.015.

Arcanjo, M.R.A., da Silva Jr., I.J., Cavalcante Jr., C.L., Iglesias, J., Morales, G., Paniagua, M., Melero, J.A., Vieira, R.S., 2020. Glycerol valorization: conversion to lactic acid by heterogeneous catalysis and separation by ion exchange chromatography. Biofuels, Bioproducts and Biorefining 14, 357–370. https://doi.org/10.1002/bbb.2055.

Arenillas, A., Moreno, A.H., Calvo, E.G., Rey-Raap, N., Menéndez, J.A., 2013. Microwave-induced Synthesis and Curing of RF-Polymers, pp. 151–154.

Belousov, A.S., Suleimanov, E.V., 2021. Application of metal–organic frameworks as an alternative to metal oxide-based photocatalysts for the production of industrially important organic chemicals. Green Chem. 23, 6172–6204. https://doi.org/10.1039/D1GC01690C.

Boudou, J.P., Chehimi, M., Broniek, E., Siemieniewska, T., Bimer, J., 2003. Adsorption of H2S or SO2 on an activated carbon cloth modified by ammonia treatment. Carbon 41, 1999–2007. https://doi.org/10.1016/S0008-6223(03)00210-0.

Bulushev, D.A., Chuvilin, A.L., Sobolev, V.I., Stolyarova, S.G., Shubin, Y.V., Asanov, I.P., Ishchenko, A.V., Magnani, G., Riccò, M., Okotrub, A.V., Bulusheva, L.G., 2017. Copper on carbon materials: stabilization by nitrogen doping. J. Mater. Chem. A 5, 10574–10583. https://doi.org/10.1039/C7TA02282D.

Canal-Rodríguez, M., Arenillas, A., Rey-Raap, N., Ramos-Fernández, G., Martín-Gullón, I., Menéndez, J.A., 2017. Graphene-doped carbon xerogel combining high electrical conductivity and surface area for optimized aqueous supercapacitors. Carbon 118, 291–298. https://doi.org/10.1016/j.carbon.2017.03.059.

Chen, X., Shen, Y.-F., Suib, S., O'Young, C.L., 2001. Catalytic decomposition of 2-propanol over different metal-cation-doped OMS-2 materials. J. Catal. 197, 292–302. https://doi.org/10.1006/jcat.2000.3063.

Chen, K., Bao, Z., Du, A., Zhu, X., Shen, J., Wu, G., Zhang, Z., Zhou, B., 2012. One-pot synthesis, characterization and properties of acid-catalyzed resorcinol/formaldehyde cross-linked silica aerogels and their conversion to hierarchical porous carbon monoliths. J. Sol. Gel Sci. Technol. 62, 294–303. https://doi.org/10.1007/s10971-012-2722-x.

Cheng, X., Shen, Z., Jiao, L., Yang, L., Wang, X., Wu, Q., Hu, Z., 2021. Tuning metal catalysts via nitrogen-doped nanocarbons for energy chemistry: from metal nanoparticles to single metal sites. EnergyChem 3, 100066. https://doi.org/10.1016/j.enchem.2021.100066.

Chernyak, S.A., Ivanov, A.S., Arkhipova, E.A., Shumyantsev, A.V., Strokova, N.E., Maslakov, K.I., Savilov, S.V., Lunin, V.V., 2019. Mechanism and kinetics of decomposition of N-containing functional groups in few-layer graphene nanoflakes. Appl. Surf. Sci. 484, 228–236. https://doi.org/10.1016/j.apsusc.2019.04.077.

Demirel-Gülen, S., Lucas, M., Claus, P., 2005. Liquid phase oxidation of glycerol over carbon supported gold catalysts. Catal. Today 102–103, 166–172. https://doi.org/10.1016/j.cattod.2005.02.033.

Deng, X., Dodekatos, G., Pupovac, K., Weidenthaler, C., Schmidt, W.N., Schüth, F., Tüysüz, H., 2015. Pseudomorphic generation of supported catalysts for glycerol oxidation. ChemCatChem 7, 3832–3837. https://doi.org/10.1002/cctc.201500703.

Deshmukh, P., Peshwe, D., Pathak, S., 2012. FTIR and TGA analysis in relation with the % crystallinity of the SiO_2 obtained by burning rice husk at various temperatures. AMR (Adv. Magn. Reson.) 585, 77–81. https://dx.doi.org/10.4028/www.scientific.net/AMR.585.77.

Djukic-Vukovic, A., Mladenović, D., Jasna, I., Pejin, J., Mojovic, L., 2019. Towards sustainability of lactic acid and poly-lactic acid polymers production. Renew. Sustain. Energy Rev. 108, 238–252. https://doi.org/10.1016/j.rser.2019.03.050.

Figueiredo, J.L., Sousa, J.P.S., Orge, C.A., Pereira, M.F.R., Órfão, J.J.M., 2011. Adsorption of dyes on carbon xerogels and templated carbons: influence of surface chemistry. Adsorption 17, 431–441. https://doi.org/10.1007/s10450-010-9272-8.

Flores-López, S.L., Montes-Morán, M.A., Arenillas, A., 2021. Carbon/silica hybrid aerogels with controlled porosity by a quick one-pot synthesis. J. Non-Cryst. Solids 569, 120992. https://doi.org/10.1016/j.jnoncrysol.2021.120992.

Flores-López, S.L., Gómez González, N., Arenillas, A., Cadus, L.E., Morales, M.R., 2024. Role of the surface chemistry of carbon xerogel-based supports and Cu catalysts in the oxidation reaction of glycerol. J. Ind. Eng. Chem. 130, 657–672. https://doi.org/10.1016/j.jiec.2023.10.039.

Friedel Ortega, K., Arrigo, R., Frank, B., Schlögl, R., Trunschke, A., 2016. Acid–base properties of N-doped carbon nanotubes: a combined temperature-programmed desorption, X-ray photoelectron spectroscopy, and 2-propanol reaction investigation. Chem. Mater. 28, 6826–6839. https://doi.org/10.1021/acs.chemmater.6b01594.

Fu, T., Wang, X., Zheng, H., Li, Z., 2017. Effect of Cu location and dispersion on carbon sphere supported Cu catalysts for oxidative carbonylation of methanol to dimethyl carbonate. Carbon 115, 363–374. https://doi.org/10.1016/j.carbon.2017.01.004.

Fuentes-Perujo, D., Santamaría-González, J., Mérida-Robles, J., Rodríguez-Castellón, E., Jiménez-López, A., Maireles-Torres, P., Moreno-Tost, R., Mariscal, R., 2006. Evaluation of the acid properties of porous zirconium-doped and undoped silica materials. J. Solid State Chem. 179, 2182–2189. https://doi.org/10.1016/j.jssc.2006.04.018.

Gervasini, A., Auroux, A., 1991. Acidity and basicity of metal oxide surfaces II. Determination by catalytic decomposition of isopropanol. J. Catal. 131, 190–198. https://doi.org/10.1016/0021-9517(91)90335-2.

Gervasini, A., Manzoli, M., Martra, G., Ponti, A., Ravasio, N., Sordelli, L., Zaccheria, F., 2006. Dependence of copper species on the nature of the support for dispersed CuO catalysts. J. Phys. Chem. B 110, 7851–7861. https://doi.org/10.1021/jp056604c.

González, N.G., Larrégola, S., Pereira, F., Cadus, L.E., Morales, M.R., 2021. Surface Acid Functionalization of Activated Carbons and its Influence in the Copper-Support Interactions, p. 7.

Gorgulho, H., Gonçalves, F., Pereira, M., Figueiredo, J., 2009. Synthesis and characterization of nitrogen-doped carbon xerogels. Carbon 47, 2032–2039. https://doi.org/10.1016/j.carbon.2009.03.050.

Haider, A., Chaturvedi, N., 2023. An energy-efficient and cleaner production of hydrogen by steam reforming of glycerol using Aspen Plus. Int. J. Hydrogen Energy 49. https://doi.org/10.1016/j.ijhydene.2023.09.089.

Hotová, G., Slovák, V., Soares, O.S.G.P., Figueiredo, J.L., Pereira, M.F.R., 2018. Oxygen surface groups analysis of carbonaceous samples pyrolysed at low temperature. Carbon 134, 255–263. https://doi.org/10.1016/j.carbon.2018.03.067.

Hu, X., Lu, J., Liu, Y., Chen, L., Zhang, X., Wang, H., 2023. Sustainable catalytic oxidation of glycerol: a review. Environ. Chem. Lett. 21 https://doi.org/10.1007/s10311-023-01608-z.

Inagaki, M., Toyoda, M., Soneda, Y., Morishita, T., 2018. Nitrogen-doped carbon materials. Carbon 132, 104–140. https://doi.org/10.1016/j.carbon.2018.02.024.

Jaiswal, S., Maurya, S., Sharma, Y.C., 2023. Studies on role of support metal in glycerol conversion to glycerol carbonate through Mg/MnO2 and Mg/CuO heterogeneous catalyst. Mol. Catal. 546, 113243 https://doi.org/10.1016/j.mcat.2023.113243.

Kaloudas, D., Pavlova, N., Penchovsky, R., 2021. Lignocellulose, algal biomass, biofuels and biohydrogen: a review. Environ. Chem. Lett. 19, 2809–2824. https://doi.org/10.1007/s10311-021-01213-y.

Kang, D.-S., Lee, S.-M., Lee, S.-H., Roh, J.-S., 2018. X-ray diffraction analysis of the crystallinity of phenolic resin-derived carbon as a function of the heating rate during the carbonization process. Carbon Letters 27, 108–111. https://doi.org/10.5714/CL.2018.27.108.

Kaur, A., Chahal, P., Hogan, T., 2016. Selective fabrication of SiC/Si diodes by excimer laser under ambient conditions. IEEE Electron. Device Lett. 37, 1. https://doi.org/10.1109/LED.2015.2508479, 1.

Koranian, P., Huang, Q., Dalai, A.K., Sammynaiken, R., 2022. Chemicals production from glycerol through heterogeneous catalysis: a review. Catalysts 12, 897. https://doi.org/10.3390/catal12080897.

Lakshmanan, P., Upare, P.P., Le, N.-T., Hwang, Y.K., Hwang, D.W., Lee, U.-H., Kim, H.R., Chang, J.-S., 2013. Facile synthesis of CeO2-supported gold nanoparticle catalysts for selective oxidation of glycerol into lactic acid. Appl. Catal. Gen. 468, 260–268. https://doi.org/10.1016/j.apcata.2013.08.048.

Loureiro, J.M., Kartel, M.T., 2006. Combined and Hybrid Adsorbents: Fundamentals and Applications. Springer Science & Business Media.

Luo, Z., Zhu, Z., Xiao, R., Chu, D., 2023. Selective production of 1,2-propanediol or 1,3-propanediol from glycerol hydrogenolysis over transition metal doped Pt/TiO2. Chem. Asian J. 18, e202201046 https://doi.org/10.1002/asia.202201046.

Mager, N., Meyer, N., Léonard, A.F., Job, N., Devillers, M., Hermans, S., 2014. Functionalization of carbon xerogels for the preparation of palladium supported catalysts applied in sugar transformations. Appl. Catal. B Environ. 148–149, 424–435. https://doi.org/10.1016/j.apcatb.2013.11.028.

Majumdar, A., Das, S., Shripathi, T., Hippler, R., 2012. Chemical synthesis and surface morphology of amorphous hydrogenated carbon nitride film deposited by N2/CH4 dielectric barrier discharge plasma. Compos. Interfac. 19 https://doi.org/10.1080/15685543.2012.699751.

Mäki-Arvela, P., Simakova, I.L., Salmi, T., Murzin, D.Y., 2014. Production of lactic acid/lactates from biomass and their catalytic transformations to commodities. Chem Rev 114, 1909–1971. https://doi.org/10.1021/cr400203v.

Montes-Morán, M.A., Menéndez, J.A., Fuente, E., Suárez, D., 1998. Contribution of the basal planes to carbon basicity: an ab initio study of the H3O+−π interaction in cluster models. J. Phys. Chem. B, 5595–5601. https://www.academia.edu/7079638/Contribution_of_the_Basal_Planes_to_Carbon_Basicity_An_Ab_Initio_Study_of_the_H_3_O_%CF%80_Interaction_in_Cluster_Models. (Accessed 19 February 2024).

Morawa Eblagon, K., Rey-Raap, N., Figueiredo, J.L., Pereira, M.F.R., 2021. Relationships between texture, surface chemistry and performance of N-doped carbon xerogels in the oxygen reduction reaction. Appl. Surf. Sci. 548, 149242 https://doi.org/10.1016/j.apsusc.2021.149242.

Moreno, A.H., Arenillas, A., Calvo, E.G., Bermúdez, J.M., Menéndez, J.A., 2013. Carbonisation of resorcinol–formaldehyde organic xerogels: effect of temperature, particle size and heating rate on the porosity of carbon xerogels. J. Anal. Appl. Pyrol. 100, 111–116. https://doi.org/10.1016/j.jaap.2012.12.004.

Pérez-Cadenas, M., Moreno-Castilla, C., Carrasco-Marín, F., Pérez-Cadenas, A.F., 2009. Surface chemistry, porous texture, and morphology of N-doped carbon xerogels. Langmuir 25, 466–470. https://doi.org/10.1021/la8027786.

Razali, N., Abdullah, A.Z., 2017. Production of lactic acid from glycerol via chemical conversion using solid catalyst: a review. Appl. Catal. Gen. 543, 234–246. https://doi.org/10.1016/j.apcata.2017.07.002.

Rey-Raap, N., Angel Menéndez, J., Arenillas, A., 2014a. RF xerogels with tailored porosity over the entire nanoscale. Microporous Mesoporous Mater. 195, 266–275. https://doi.org/10.1016/j.micromeso.2014.04.048.

Rey-Raap, N., Angel Menéndez, J., Arenillas, A., 2014b. Simultaneous adjustment of the main chemical variables to fine-tune the porosity of carbon xerogels. Carbon 78, 490–499. https://doi.org/10.1016/j.carbon.2014.07.030.

Rinaudo, M.G., Beltrán, A.M., Fernández Camacho, A., Cadús, L.E., Morales, M.R., 2022. Pd supported on defective TiO2 polymorphic mixtures: effect of metal-support interactions upon glycerol selective oxidation. https://doi.org/10.1016/j.rineng.2022.100737.

Robinson, E., Ross, R.A., 1970. Studies of the pore structures of silica gels by electron microscopy and low-temperature nitrogen adsorption. Can. J. Chem. 48, 2210–2214. https://doi.org/10.1139/v70-369.

Sahai, N., 2002. Is silica really an anomalous oxide? Surface acidity and aqueous hydrolysis revisited. Environ. Sci. Technol. 36, 445–452. https://doi.org/10.1021/es010850u.

Sarkodie, B., Hu, Y., Bi, W., Jiang, J., Li, C., 2021. Promotional effects of CuxO on the activity of Cu/ZnO catalyst toward efficient CO oxidation. Appl. Surf. Sci. 548, 149241 https://doi.org/10.1016/j.apsusc.2021.149241.

Sato, S., 2021. Application of glyceric acid to bio-related functional materials and improvement of microbial production. J. Oleo Sci. 70, 289–295. https://doi.org/10.5650/jos.ess20307.

Segovia-Sandoval, S.J., Pastrana Martínez, L.M., Ocampo-Pérez, R., Morales Torres, S., Berber Mendoza, M.S., Carrasco Marín, F., 2019. Synthesis and characterization of carbon xerogel/graphene hybrids as adsorbents for metronidazole pharmaceutical removal: effect of operating parameters. https://doi.org/10.1016/j.seppur.2019.116341.

Shan, J., Liu, H., Lu, K., Zhu, S., Li, J., Wang, J., Fan, W., 2020. Identification of the dehydration active sites in glycerol hydrogenolysis to 1,2-propanediol over Cu/SiO2 catalysts. J. Catal. 383, 13–23. https://doi.org/10.1016/j.jcat.2019.12.032.

Shan, J., Xue, Y., Wang, D., Chen, Z., Zhu, S., 2022. Direct production of ethanol with high yield from glycerol via synergistic catalysis by Pd/CoOx and Cu/SBA-15. Appl. Catal. B Environ. 302, 120870 https://doi.org/10.1016/j.apcatb.2021.120870.

Siburian, R., Sihotang, H., Raja, S.L., Supeno, M., Simanjuntak, C., 2018. New route to synthesize of graphene nano sheets. Orient. J. Chem. 34, 182–187. https://www.orientjchem.org/vol34no1/new-route-to-synthesize-of-graphene-nano-sheets/. (Accessed 31 March 2024).

Taib, N.-A., Rahman, M., Huda, D., Kuok, K., Hamdan, S., Bakri, M.K., Julaihi, M., Khan, A., 2022. A review on poly lactic acid (PLA) as A biodegradable polymer. Polym. Bull. 1, 1–35. https://doi.org/10.1007/s00289-022-04160-y.

Thommes, M., Kaneko, K., Neimark, A.V., Olivier, J.P., Rodriguez-Reinoso, F., Rouquerol, J., Sing, K.S.W., 2015. Physisorption of gases, with special reference to the evaluation of surface area and pore size distribution (IUPAC Technical Report). Pure Appl. Chem. 87, 1051–1069. https://doi.org/10.1515/pac-2014-1117.

Villa, A., Campisi, S., Mohammed, K.M.H., Dimitratos, N., Vindigni, F., Manzoli, M., Jones, W., Bowker, M., Hutchings, G.J., Prati, L., 2015. Tailoring the selectivity of glycerol oxidation by tuning the acid–base properties of Au catalysts. Catal. Sci. Technol. 5, 1126–1132. https://doi.org/10.1039/C4CY01246A.

Wu, C.-K., Yin, M., O'Brien, S., Koberstein, J.T., 2006. Quantitative analysis of copper oxide nanoparticle composition and structure by X-ray photoelectron spectroscopy. Chem. Mater. 18, 6054–6058. https://doi.org/10.1021/cm061596d.

Xiong, H., Moyo, M., Rayner, M.K., Jewell, L.L., Billing, D.G., Coville, N.J., 2010. Autoreduction and catalytic performance of a cobalt fischer–tropsch synthesis catalyst supported on nitrogen-doped carbon spheres. ChemCatChem 2, 514–518. https://doi.org/10.1002/cctc.200900309.

Xu, S., Tian, Q., Xiao, Y., Zhang, W., Liao, S., Li, J., Hu, C., 2022. Regulating the competitive reaction pathway in glycerol conversion to lactic acid/glycolic acid selectively. J. Catal. 413, 407–416. https://doi.org/10.1016/j.jcat.2022.07.003.

Yan, X., Xu, T., Chen, G., Yang, S., Liu, H., Xue, Q., 2004. Preparation and characterization of electrochemically deposited carbon nitride films on silicon substrate. J. Phys. D Appl. Phys. 37, 1–7. https://doi.org/10.1088/0022-3727/37/6/015.

Yang, B., Yu, C., Yu, Q., Zhang, X., Li, Z., Lei, L., 2015. N-doped carbon xerogels as adsorbents for the removal of heavy metal ions from aqueous solution. RSC Adv. 5, 7182–7191. https://doi.org/10.1039/C4RA12441C.

Yu, J., Guo, M., Muhammad, F., Wang, A., Zhang, F., Li, Q., Zhu, G., 2014. One-pot synthesis of highly ordered nitrogen-containing mesoporous carbon with resorcinol–urea–formaldehyde resin for CO2 capture. Carbon 69, 502–514. https://doi.org/10.1016/j.carbon.2013.12.058.

Yu, X.-M., Ke, Y., Wang, X., Liu, H., Yuan, H., 2024. MOFs-Derived MnxOyCz supported bimetallic Au–Pt catalyst for the catalytic oxidation of glycerol to glyceric acid. Chem. Mater. 36, 1737–1752. https://doi.org/10.1021/acs.chemmater.3c03111.

Yuan, J., Zhang, J.-J., Yang, M.-P., Meng, W.-J., Wang, H., Lu, J.-X., 2018. CuO nanoparticles supported on TiO2 with high efficiency for CO2 electrochemical reduction to ethanol. Catalysts 8, 171. https://doi.org/10.3390/catal8040171.

Žalac, S., Kallay, N., 1992. Application of mass titration to the point of zero charge determination. J. Colloid Interface Sci. 149, 233–240. https://doi.org/10.1016/0021-9797(92)90408-E.

Zhang, P., Wang, Q.-N., Yang, X., Wang, D., Li, W.-C., Zheng, Y., Chen, M., Lu, A.-H., 2016. A highly porous graphitic-N rich carbon stabilized copper nanocatalysts for efficient ethanol dehydrogenation. ChemCatChem 9. https://doi.org/10.1002/cctc.201601373.

Zhou, C.-H., Beltramini, J.N., Lin, C.-X., Xu, Z.-P., Max, G.Q., Lu, Tanksale, A., 2011. Selective oxidation of biorenewable glycerol with molecular oxygen over Cu-containing layered double hydroxide-based catalysts. Catal. Sci. Technol. 1, 111–122. https://doi.org/10.1039/C0CY00018C.

Zhou, X., Yan, H., Feng, X., Zhao, H., Liu, Y., Chen, X., Chen, D., Yang, C., 2021. Producing glyceric acid from glycerol via integrating vacuum dividing wall columns: conceptual process design and techno-economic-environmental analysis. Green Chem. 23, 3664–3676. https://doi.org/10.1039/D1GC00327E.